ACS Biomaterials SCIENCE & ENGINEERING

pubs.acs.org/journal/abseba

Article

Rapid Prototyping of Multilayer Microphysiological Systems

Sanjin Hosic, Adam J. Bindas, Marissa L. Puzan, Will Lake, Jonathan R. Soucy, Fanny Zhou, Ryan A. Koppes, David T. Breault, Shashi K. Murthy, and Abigail N. Koppes*

Cite This: *ACS Biomater. Sci. Eng.* 2021, 7, 2949−2963

Read Online

ACCESS | Metrics & More | Article Recommendations | Supporting Information

ABSTRACT: Microfluidic organs-on-chips aim to realize more biorelevant in vitro experiments compared to traditional two-dimensional (2D) static cell culture. Often such devices are fabricated via poly(dimethylsiloxane) (PDMS) soft lithography, which offers benefits (e.g., high feature resolution) along with drawbacks (e.g., prototyping time/costs). Here, we report benchtop fabrication of multilayer, PDMS-free, thermoplastic organs-on-chips via laser cut and assembly with double-sided adhesives that overcome some limitations of traditional PDMS lithography. Cut and assembled chips are economical to prototype ($2 per chip), can be fabricated in parallel within hours, and are Luer compatible. Biocompatibility was demonstrated with epithelial line Caco-2 cells and primary human small intestinal organoids. Comparable to control static Transwell cultures, Caco-2 and organoids cultured on chips formed confluent monolayers expressing tight junctions with low permeability. Caco-2 cells-on-chip differentiated ∼4 times faster, including increased mucus, compared to controls. To demonstrate the robustness of cut and assemble, we fabricated a dual membrane, trilayer chip integrating 2D and 3D compartments with accessible apical and basolateral flow chambers. As proof of concept, we cocultured a human, differentiated monolayer and intact 3D organoids within multilayered contacting compartments. The epithelium exhibited 3D tissue structure and organoids expanded close to the adjacent monolayer, retaining proliferative stem cells over 10 days. Taken together, cut and assemble offers the capability to rapidly and economically manufacture microfluidic devices, thereby presenting a compelling fabrication technique for developing organs-on-chips of various geometries to study multicellular tissues.

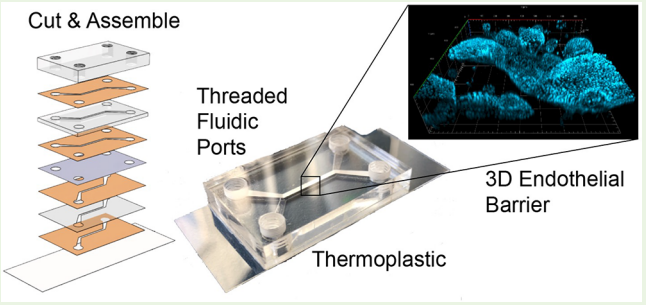

KEYWORDS: *gut chip, organ-on-chip, fabrication, economical, thermoplastic, adhesive, intestinal organoid, primary epithelium, patient-derived cells*

INTRODUCTION

Two-dimensional (2D) tissue culture originated one century ago[1] and remains invaluable for studying biology and developing therapeutics. Nevertheless, 2D cultures inaccurately represent native tissues. In vivo, continuous nutrient supply and waste product removal occurs via luminal flow of the circulatory and lymphatic systems, which maintain a homeostatic steady state.[2] Native cells experience physical cues such as fluid shear forces[3,4] or multilateral mechanical stretching[4] and chemical cues from heterogeneous tissue−tissue interfaces.[5,6] Microfluidic organs-on-chips are cell culture models that recapitulate heterogeneous tissue−tissue interfaces and integrate continuous media perfusion to maintain biochemical homeostasis and flow-induced shear stress.[7,8]

The predominant embodiment of organs-on-chip, or microphysiological systems, is a bilayer design featuring two channels interfaced by a porous membrane[9−20] or hydrogel.[21,22] Culturing different cell types on opposing membrane surfaces or in adjacent channels mimics heterogeneous tissue−tissue interfaces. The bilayer chip has been used to model the blood−brain barrier,[17] the hematopoietic stem cell niche,[16] the gut microbiome−epithelial−immune interface,[12,15] the lung alveolar−capillary interface,[10] and the placental barrier.[14] Future organs-on-chips integrating patient-derived cells may enable personalized medicine.[13] Interconnecting multiple organs-on-chips via an artificial circulatory system, termed body-on-a-chip, may permit in vitro pharmacokinetics.[23−26] Despite these advances, organs-on-chips have been concentrated among bioengineering research groups and have yet to transition to mass clinical or diagnostic applications. Chip automation and parallelization remains challenging, and complex, multilayered (>2 layers) chips are limited.

Facile, rapid, economic, and reliable organ-on-chip fabrication would promote interdisciplinary adoption and technological development. Organs-on-chips are most frequently

Special Issue: Beyond PDMS and Membranes: New Materials for Organ-on-a-Chip Devices

Received: February 6, 2020
Accepted: May 20, 2020
Published: May 20, 2020

https://dx.doi.org/10.1021/acsbiomaterials.0c00190
ACS Biomater. Sci. Eng. 2021, 7, 2949−2963

fabricated via poly(dimethylsiloxane) (PDMS) soft lithography.[10,12,27−29] The many advantages of PDMS organs-on-chips include high feature resolution, biocompatibility, optical transparency, and gas permeability enabling culture oxygenation and pH control in standard CO_2 incubators.[30] But, PDMS organs-on-chips have several drawbacks. PDMS's gas permeability[30] prohibits O_2 tension control, which while notably beneficial in some applications, is necessary for recapitulation of hypoxic tissue conditions, as seen in the small intestinal lumen.[31] PDMS gas permeability can be harnessed by hypoxic incubators,[32] surface treatments, cellular metabolism, and controlled permeability of tubing and equpiment.[20,33] PDMS's water vapor permeability[30] results in evaporation induced bubble formation, which can block flow and impact cell fate and viability.[34] PDMS can absorb hydrophobic or small molecules,[30] complicating drug pharmacokinetic studies. Drug loss in PDMS devices and mixing can be minimized by varying drug properties such as charge or molecular weight, design parameters, and flow conditions, however biological constraints may impact parameters as well.[33,35] While PDMS easily bonds to both itself and glass via plasma activation, bonding to polymers requires additional processing such as silanization.[36] PDMS soft lithography requires significant microfabrication training and capital infrastructure.[9] Moreover, initial prototyping may require multiple iterations, and lithographic mold fabrication can be prohibitively expensive ($150−500 per design from third party manufacturers).

Other investigators have 3D printed microfluidic cell culture models,[37,38] but these single channel devices do not integrate membranes for recapitulating tissue−tissue interfaces. Recently, advances from the Ingber team have utilized 3D printing of molds for fabricating scalable PDMS bilayer organ chips, circumventing many of the aforementioned limitations in cost of capital equipment of traditional soft lithography.[39] Rapid and economic microfluidic devices were fabricated with laser or razor cut thermoplastic or adhesive sheets, though these were typically analytical microdevices,[40−42] and not cell culture platforms. A recent work comparing adhesive tape based cell culture platforms against traditional 96-well plates and analogous PDMS platforms found that tape based platforms compared favorably in regards to cell viability and morphology across three different human breast cancer cell lines.[43] This study highlighted additional benefits of tape-based cell culture platforms such as economical fabrication, high throughput, and facile bonding of disparate materials such as polystyrene and glass. However, cell culture experiments were limited to 24 h and immortalized human cell lines and performed on 2D substrates, either glass or polystyrene.[43] Therefore, in this study, we aimed to fabricate multilayered, membrane integrated organs-on-chips for long-term primary cell culture with tailorable geometries without traditional PDMS soft lithography.

A single-layer epithelium lines the intestinal wall and forms the rate-limiting barrier to drug absorption.[44] Therefore, oral drug absorption in humans can be approximated using an in vitro differentiated, intestinal epithelium.[45] The human colon carcinoma Caco-2 cell line cultured on static permeable supports differentiates into a monolayer with some features of the native small intestine.[46] Organ-on-chip technology was used to develop Caco-2 models with greater fidelity to human intestinal structure and function.[11,12,28,47] Nevertheless, the immortalized Caco-2 cell line has limited genetic similarity to human intestinal epithelium. Recent advances in intestinal biology have enabled primary human cultures containing intestinal stem cells (self-renewal), Paneth cells (antimicrobial peptide secretion), goblet cells (mucus production), enteroendocrine cells (hormone production), and enterocytes (absorption) via organoid technology.[48,49] Primary, three-dimensional (3D) organoids are established from biopsy- or resection-derived intestinal stem cells embedded in Matrigel.[48] While intestinal organoids are genetically and phenotypically more closely related to the native epithelium, organoids form closed lumens that complicate intestinal transport studies. To enable luminal access, researchers cultured primary intestinal monolayers on static permeable supports,[50−52] but these models failed to emulate the native 3D tissue structure. More recently, primary intestinal monolayers exhibiting crypt-villus like tissue organization were formed on microengineered scaffolds[53] and organs-on-chips.[13,54] Thus, in this study, we too aimed to integrate primary intestinal monolayers and organoids on organ chips.

Here, we describe a "cut and assemble" process for manufacturing thermoplastic organs-on-chips. Most importantly, our technique produced multilayer devices with integrated polymeric membranes and Luer fluidic interfaces faster than soft lithography (hours versus days) at minimal cost (~$2 per device) without specialized bonding. The resulting biocompatible, thermoplastic chips are water vapor and gas impermeable, thereby eliminating evaporation-induced bubble formation while potentially enabling O_2 tension control. Use of thermoplastics over PDMS in microphysiological systems has also been demonstrated to both adsorb or absorb less hydrophobic molecules.[55] The cut and assemble manufacturing technique was validated by reengineering a recently described gut-on-a-chip[12,28] using Caco-2 cells and primary human intestinal organoids. Caco-2 cells and primary organoids cultured in a bilayer chip formed confluent monolayers expressing tight junctions and low permeability comparable to static Transwell controls. Furthermore, Caco-2 cultures on-chip differentiated 4 times faster toward the enterocyte phenotype as compared to controls and produced mucus, corroborating previously published results.[56] We integrated primary intestinal monolayers and 3D intact organoids in a dual membrane, trilayer organ chip. Monolayers exhibited 3D tissue structure spanning 10^2 μm in height, and organoids formed typical cystic structures in close proximity to monolayers, potentially enabling paracrine signaling. The rapid, benchtop, fabrication process presented here has great potential to enable microphysiological modeling of multicellular tissues, 3D cell culture, and the study of paracrine signaling. Although the presented experiments integrate existing technologies such as primary organoid culture, membrane-integrated organs-on-chips, and microfluidic device fabrication via adhesive films, they represent a scientific work that enables wider adoption of organs-on-chips and drives technological development.

EXPERIMENTAL SECTION

Chip Design and Fabrication. In contrast to practically all previous iterations of gut-on-a-chip, the bilayer chip discussed herein was fabricated without lithography. The rapid cut and assemble manufacturing process required only a laser cutter/engraver, double-sided adhesive tape, and sheets of poly(methyl methacrylate) (PMMA) and polyester (PET). First, all chip layers were simultaneously designed using CAD software (SOLIDWORKS,

https://dx.doi.org/10.1021/acsbiomaterials.0c00190
ACS Biomater. Sci. Eng. 2021, 7, 2949−2963

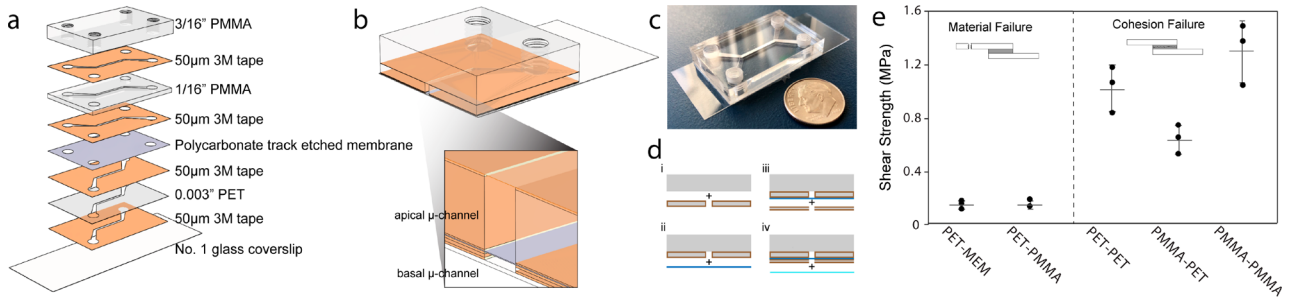

Figure 1. Laser cut and assembled membrane integrated bilayered organ chip. (a) A schematic showing the integration of nine discrete layers to form a bilayered organ chip. (b) A schematic of an assembly cutaway view of the bilayered organ chip showing the inner apical and basal microchannels. (c) A photograph of the bilayered organ chip composed of clear PMMA, acrylic adhesive, polycarbonate track etched membrane, and glass coverslip. (d) Five layers are aligned and irreversibly bonded in four steps to form the apical and basal channels separated by a polycarbonate track etched membrane with a pore diameter of 1.0 μm. (e) Shear strength of bonded layers from a single-lap shear test indicate mechanical integrity to prevent burst or leaking (horizontal bar = mean, error bars = S.D.).

Waltham, MA). Then, a laser cutter (Epilog Zing 16, Epilog Laser, Golden, CO) was used to transfer the CAD design to the various materials. The 3/16″ PMMA upper layer (McMaster-Carr, Robbinsville, NJ) featured four circular through holes, which served as fluidic inlets and outlets for both the upper and bottom fluidic layers. The second layer was comprised of a 0.003″ polyester or a 1/16″ PMMA sheet (McMaster-Carr, Robinsville, NJ), which was sandwiched between 50-μm-thick double-sided adhesive tape (966 adhesive, 3M, Maplewood, Minnesota). This 1-mm-wide channel served as the upper fluidic channel used for cell culture. The circular inlets and outlets matched the diameter of the through-holes in the uppermost 3/16″ PMMA sheet. The third layer, a polycarbonate (PC), track etched membrane with 1.0 μm diameter pores (cat no. 7091−4710, GE Healthcare, Marlborough, MA), featured two circular through-holes with identical diameters as the previous layers. The membrane through-holes enabled fluidic access to the bottom fluidic channel. The fourth layer was comprised of a 0.003″ polyester sheet sandwiched between 50 μm double-sided adhesive tape. The fifth and final layer was a no. 1 glass coverslip. During laser cutting, the protective paper lining on both the PMMA sheets and the double-sided adhesives minimized exposing the materials to burn products. Post laser cutting, 10−32 UNF threads were hand tapped in each of the circular through-holes on the top PMMA sheet. Next, the protective paper lining on both upper and lower PMMA sheets was removed, and the plastics were serial cleaned by rinsing with deionized water, Contrad 70 detergent (Fisher), deionized water, and isopropyl alcohol and then dried with compressed nitrogen. The laser cut layers were then assembled layer by layer using a custom jig to facilitate hole and channel alignment. The two layers of double-sided adhesive tape served as the apical and basal fluidic channels and simultaneously bonded the entire chip (Figure 1a−c). Post assembly, the devices were stored under a vacuum at 37 °C overnight in order to eliminate outgassing-induced bubble formation. Threaded, polypropylene, male Luer lock fittings (cat no. EW-45518-84, Cole-Parmer, Vernon Hills, IL) were connected to the chip via the threaded inlets and outlets. Barbed PC connectors with female Luer lock connections (cat no. 11733, Qosina, Ronkonkoma, NY) were connected to the chip. Tubing (cat no. SC-95802-01, silicone, ID 1/32″, OD 3/32″, Cole-Parmer, Vernon Hills, IL) was fitted over the barbed ends to perfuse culture medium through the device.

The bilayer chip was modified for use with organoid derived primary human intestinal epithelial cells to enable seeding at a lower cell concentration while enabling confluent monolayer formation postseeding. The top fluidic channel was replaced with a 1/16″ PMMA sheet sandwiched between 50-μm-thick double-sided adhesive tape (966 adhesive, 3M, Maplewood, Minnesota) for a final channel height of 1.6876 mm. Furthermore, the top 3/16″ PMMA cover was not bonded until the day of use, at which point the PC membrane was treated with oxygen plasma (50 W, 30 s, March PX-250 Plasma System).

A dual-membrane trilayer chip was designed and fabricated for coculture of 2D primary monolayers and 3D organoids (Figure 6a−c). Two additional components were added to the bilayer architecture: (1) a 1/16″ PMMA sandwiched between two pieces of 50-μm-thick double-sided adhesive tape as with the 3D gel channel and (2) a PC, track-etched membrane with 30.0 μm diameter pores (cat no. PCT30047100, Sterlitech, Kent, WA).

Bond Strength of Chip Layers. To assess bond strength of 3 M 966 adhesive-bonded layers of thermoplastics, a single-lap shear test was carried out. Bonded materials were loaded to failure at a strain rate of 3 mm/min on a universal load frame (TA Instruments ElectroForce 3200). Thermoplastics were laser cut and bonded overnight under vacuum conditions and at a temperature of 37 °C in a vacuum oven (Isotemp Model 282A) assisted with pressure using binder clips (Staples 10669). Prior to bonding, membrane layers were plasma treated (Harrick Plasma PDC-001) for 1 min to recapitulate a typical fabrication process. The bonding area was fixed to a 1 cm^2 square for all samples. Lap-shear strength stress (τ) was found as the ultimate load over the cross-sectional area of the adhered joint. Investigations compared the bond strength of adhesives between all relevant materials. Each material combination was tested in triplicate.

Caco-2 Cell Culture. Caco-2 epithelial cells were obtained from the American Type Culture Collection (ATCC) and cultured in Dulbecco's Modified Eagle Medium (DMEM, cat no. 11995-065, ThermoFisher) supplemented with 10% fetal bovine serum (FBS, cat no. 35-011-CV, Corning) and 100 U/mL penicillin−streptomycin (cat no. 15140122, ThermoFisher). Cells were cultured in a 37 °C, 5% CO_2 incubator. All experiments were done with Caco-2 cells between passage numbers 40 and 50.

After fabrication, the bilayer chip was sterilized via UV irradiation (300 mJ/cm^2) of the top and bottom chip surfaces (Spectrolinker XL-1000, Spectronics Corporation, Westbury, NY). All tubing and fittings were preassembled and sterilized via autoclave. Both apical and basal fluidic channels were coated with a 400 μg/mL solution of rat tail type I collagen (cat no. 354249, Corning, Corning, NY) in DMEM for at least 1 h at 37 °C inside a humidified cell culture incubator with 5% CO_2. The device and tubing were then flushed with Caco-2 culture medium via a sterile, plastic syringe. Caco-2 cells were harvested from a sub-confluent T75 flask via 0.25% Trypsin-EDTA (cat no. 25200056, ThermoFisher) and incubation at 37 °C. After cell detachment, the Trypsin-EDTA was diluted with an equal volume of cell culture media and centrifuged at 300g for 5 min at room temperature. The cells were suspended in a cell culture medium at 5 × 10^6 cells/mL. The outlet to the bottom fluidic channel was clamped, and the harvested cells were infused into the top fluidic channel via a sterile 1 mL syringe. The chips were placed in a 37 °C, 5% CO_2 cell culture incubator for 1−2 h for cell attachment. Post-attachment, culture medium was perfused through the apical channel via a syringe pump (Ph.D. 2000, Harvard Apparatus, Holliston, MA) at a rate of 0.84 uL/min. The next day, culture medium was perfused through both the apical and basal channels at a rate of 0.84 μL/min.

https://dx.doi.org/10.1021/acsbiomaterials.0c00190
ACS Biomater. Sci. Eng. 2021, 7, 2949−2963

As controls, Caco-2 cells were cultured on 0.4 μm polyester (cat no. 353095, Corning, Corning, NY) Transwell inserts in a 24 well plate. Prior to cell seeding, the insets were coated with 200 μL of the collagen solution for at least 1 h at 37 °C inside a humidified cell culture incubator with 5% CO_2. Caco-2 cells were seeded on the insets by adding 200 μL of Caco-2 cell suspension (seeding density of 2.6×10^5 cells/cm^2) and then adding 600 μL of media to the basolateral compartment. The apical and basal cell culture medium was refreshed every other day.

Organoid Culture of Biopsy Derived Intestinal Stem Cells. Deidentified endoscopic tissue biopsies were collected from grossly unaffected (macroscopically normal) areas of the duodenum in children undergoing endoscopy for gastrointestinal complaints. Informed consent and developmentally appropriate assent were obtained at Boston Children's Hospital from the donors' guardian and the donor, respectively. All methods were approved and carried out in accordance with the Institutional Review Board of Boston Children's Hospital (protocol number IRB-P00000529). Cells were cultured as 3D organoids embedded in 50 μL of Matrigel (cat no. 354230, Corning) on a 24-well plate as previously described.[57] Expansion medium (EM) for expanding intestinal organoids was prepared from a mixture of Advanced DMEM/F12 medium (cat no. 12634028, Gibco) and 50% L-WRN conditioned medium, which was prepared from L-WRN cells, as previously described.[58] This cell line produces Wnt-3A, R-spondin 3, and noggin. EM was supplemented with GlutaMAX (1×, cat no. 35050061, Gibco), HEPES (10 mM, cat no. 15630080, Gibco), Primocin (0.1 mg/mL, Invivogen), B-27 supplement (0.5×, cat no. 12587010, Gibco), N-2 supplement (0.5×, cat no. 17502048, Gibco), nicotinamide (10 mM, cat no. N0636, Sigma-Aldrich), N-acetyl cysteine (0.5 mM, cat no. A7250, Sigma-Aldrich), epidermal growth factor (50 ng/mL, cat no. 315-09, Peprotech), gastrin (50 nM, cat no. A7250, Sigma-Aldrich), A-83-01 (500 nM, cat no. SML0788, Sigma), prostaglandin E2 (10 nM, cat no. 14010, Cayman Chemical), and SB202190 (10 μM, cat no. S7067, Sigma-Aldrich). Y-27632 ROCK inhibitor (10 μM, cat no. Y0503, Sigma-Aldrich) was added to the organoid medium for the first 48 h following cell isolation or passage. The culture medium was refreshed every 48 h using 500 μL per well. Cell culture was performed in a humidified, 37 °C, 5% CO_2 incubator.

Every 7−10 days, the organoids were passaged to new 24-well plates at a ratio of 1:4−1:8 depending on culture density. Matrigel droplets were scratched off the 24-well plate using a 1000 μL pipet tip and collected into a 15 mL conical tube. The organoids were centrifuged at 500*g* for 5 min at room temperature. After aspirating the cell culture medium, the organoids were resuspended in 0.5 mM ethylenediaminetetraacetic acid (EDTA, cat no. AM9260G, Gibco) in 1× PBS and recentrifuged at 300*g* for 5 min at room temperature. After aspirating the EDTA, the organoids were resuspended in Trypsin-EDTA and incubated in a 37 °C bath for 2 min. The Trypsin-EDTA was then quenched via a 2:1 dilution with Caco-2 culture medium containing 10% FBS and the organoid suspension was triturated ∼10× using a 1000 μL pipet tip to produce single cells and small organoid fragments. The cells were pelleted at 300*g* for 5 min at room temperature. The cells were suspended in 4 °C Matrigel and replated on new 24-well plates. The plated Matrigel was incubated at 37 °C for 15 min before adding 500 μL of culture medium containing 10 μM ROCK inhibitor.

Monolayer Culture of Primary Human Intestinal Epithelial Cells. Polyester Transwell inserts in a 24-well plate were coated with 200 μL of collagen solution for at least 1 h at 37 °C inside a humidified cell culture incubator with 5% CO_2. Organoids were harvested for dissociation and monolayer seeding after 7−10 days of culture. Matrigel droplets were harvested and processed in Trypsin-EDTA as described above. The Trypsin-EDTA was then quenched via a 2:1 dilution with Caco-2 culture medium containing 10% FBS, and the organoid suspension was triturated ∼20× using a 1000 μL pipet tip to produce single cells and small organoid fragments. The cell suspension was filtered through a 40 μm cell strainer (cat no. 22-363-547, Fisher) into a 50 mL conical tube and pelleted at 300*g* for 5 min at room temperature. The cells were resuspended in EM with 10 μM ROCK inhibitor. Transwell inserts were seeded using 200 μL of cell suspension (seeding density of 9.09×10^5 viable cells/cm^2), and then 600 μL of media plus 10 μM ROCK inhibitor were added to the basolateral compartment. ROCK inhibitor was used for the first 48 h of cell culture, and the apical and basal cell culture medium was refreshed every other day. Following 2 days of culture in EM, the apical and basal media were replaced with differentiation medium (DM) containing Advanced DMEM/F12 + 20% FBS + 4 mM GlutaMAX supplement + 100 U/mL Penicillin-Streptomycin. Apical and basal DM media were replenished every 48 h.

For seeding primary human intestinal epithelial cells on bilayer chips, the cells were harvested as described above and suspended at a concentration of 10×10^6 cells/mL. Cell viability was assessed via trypan blue exclusion by incubating cells with an equal volume of 0.4% Trypan Blue Solution (15250061, ThermoFisher). The organoid dissociation method was quantified by imaging the processed cell suspension with a brightfield microscope and counting the total amount of single cells, cell doublets, cell triplets, and larger aggregates. Prior to seeding, the bilayer chip was treated with O_2 plasma (50 W, 30s, pure O_2, March PX-250 Plasma System), and the 3/16″ acrylic cover was bonded. Note that primary cell adhesion required a plasma treated membrane, whereas Caco-2 cells adhered without plasma treatment. The chip was sterilized via UV irradiation as previously described. The chip was coated with collagen solution for 2 h after which the collagen was flushed with EM medium containing 10 μM ROCK inhibitor. The cell suspension was perfused through the apical channel, and the chips were maintained under static conditions in a 37 °C humidified cell culture incubator with 5% CO_2 for 5−6 h to enable cell attachment. Then, the apical medium was perfused at 1.48 μL/min with EM medium for 3 days before changing to DM medium for 2 additional days. The basal medium was manually refreshed every 24 h, with EM and DM media, as above.

Alkaline Phosphatase Measurement. Alkaline phosphatase (AP) expression was measured using a commercial kit (AS-71109, AnaSpec, Fremont, CA). All kit components were prepared as specified by the manufacturer. Cell lysate from Transwell inserts was prepared as follows: the medium was removed, and the insets were washed two times with sterile PBS in both apical and basal compartments. Next, 200 μL of sterile 10× TrypLE Select (A1217701, ThermoFisher) was added to the apical side of each insert prior to incubation at 37 °C for ∼15 min. Cells were collected into a sterile centrifuge tube, and inserts were washed with 800 μL of sterile PBS and pelleted at 300*g* for 5 min at room temperature. The pellet was resuspended in 150 μL of AP kit supplied buffer, washed, and resuspended in 150 μL of buffer. A 10 μL aliquot of cell suspension was removed to quantify the cell number via hemocytometer. The cells were centrifuged and suspended in 0.2% Triton X-100 (AC327371000, Fisher Scientific). The cells were incubated for 10 min at 4 °C with agitation and then centrifuged at 2500*g* for 10 min at 4 °C. The supernatant was used for the AP assay. A total of 50 μL of the supernatant was moved to a well of a black, polystyrene, 96-well plate (12−566−620, Fisher Scientific). Then, 50 μL of the reaction mixture was added to each well, and the plate was manually mixed for 30 s. Following a 30 min incubation at 37 °C, 50 μL of stop solution was added to each well. The plate was manually mixed for 30 s. The fluorescence was measured via plate reader (EnSight, PerkinElmer) using 485 and 528 nm emission and excitation wavelengths, respectively. For Caco-2 on a chip, the same protocol was used except that the 10× TrypLE and the subsequent PBS wash were infused via a sterile, plastic syringe to detach cells. The actual amount of AP was interpolated using a calibration curve generated with the kit supplied AP standard.

Paracellular Permeability Measurement. The apparent permeability coefficient for tetramethylrhodamine (TRITC) labeled dextran (4.4 kDa; cat no. T1037, Sigma-Aldrich) was determined by measuring transport across the Caco-2 cell monolayer as previously described.[51] TEER values of cell monolayers were measured prior to the permeability assay, and monolayers with TEER values below 165 Ω cm^2 were not used.[44] For control Transwell cultures, 300 μL of 500 μM dextran in cell culture medium was applied to the apical

https://dx.doi.org/10.1021/acsbiomaterials.0c00190
ACS Biomater. Sci. Eng. 2021, 7, 2949−2963

compartment. A total of 100 μL was immediately sampled from the apical compartment, transferred to a black, polystyrene, 96-well plate and stored at 4 °C. Transwells were maintained in a humidified, 37 °C + 5% CO_2 incubator. Then, 100 μL aliquots were sampled from the basolateral compartment every 30 min over 3 h, and 100 μL of fresh medium preheated to 37 °C was added to replace the aliquoted volume. The fluorescence intensity of the collected basolateral samples was measured at 557 and 576 nm emission and excitation wavelengths, respectively. The interpolated dextran concentration was determined using a standard curve. The apparent permeability coefficient was calculated as specified. For Caco-2 on a chip, the dextran solution was perfused through the upper channel, and cell culture medium was perfused through the lower channel at a rate of 0.84 μL/min. Aliquots were sampled from the lower channel every hour and stored at 4 °C. The apparent permeability coefficient for Lucifer Yellow (450 Da; cat no. L0259, Sigma-Aldrich) across primary organoid derived monolayers on static inserts and bilayer chips was determined as described above.

Monolayer Morphology and Mucus Production Measurement. Cell morphology was assessed by staining F-actin, nuclei, and ZO-1 tight junction protein. Monolayers were washed and stained at room temperature. All monolayers were washed three times with PBS and fixed in 4% formaldehyde (cat no. 28906, ThermoFisher) for 20 min. Post fixation, the monolayers were permeabilized in 0.1% Triton X-100 for 20 min and blocked overnight in 2% bovine serum albumin solution (BSA, cat no. 97061−416 VWR). The next day, the monolayers were stained with anti-ZO-1 antibody (1:200, 1 h, cat no. 339188, ThermoFisher), phalloidin (1:500, 1 h, cat no. A22287, ThermoFisher), and DAPI (1:1000, 10 min, cat no. D1306, ThermoFisher) diluted in 1% BSA solution. Transwell membranes were isolated and mounted on a standard glass slide and coverslip with Gold Antifade Mountant (cat no. P36931, ThermoFisher).

Mucus production was assessed by alcian blue and immunostaining for MUC2 protein. Monolayers were washed and stained at room temperature. For alcian blue staining, monolayers were washed three times with PBS and fixed with 4% formaldehyde for 20 min. Next, the cell monolayers were washed three times with PBS and stained for 20 min with a 1% alcian blue solution in 3% acetic acid (pH = 2.5, cat no. 50-319-30, Fisher Scientific) that was filtered via a 0.1 μm syringe filter. Post staining, monolayers were washed five times with PBS. For MUC2 immunostaining, the monolayers were washed, fixed, permeabilized, and blocked as previously described. Mucin was detected via an antimucin 2 primary antibody (1:200, 1 h, cat no. PA1-23786, ThermoFisher) and an Alexa Fluor 647 secondary antibody (1:1000, 1 h, A-21244, ThermoFisher). For monolayers in the bilayer chip, the protocol remained the same, but washes and stains were applied via syringe pumps to minimize damage to the monolayer.

The trilayer chip was stained as follows. All steps were performed at room temperature, and all washes and stains were applied to both apical and basal channels via syringe pump to minimize damage to the monolayer. The chip was washed with 500 μL of PBS followed by 4% formaldehyde for 30 min. The chip was washed with 500 μL of PBS prior to application of 0.1% Triton X-100 for 30 min. The chip was then washed with 2.5% goat serum applied via syringe pump overnight. The chip was washed with 500 μL of PBS prior to the addition of a cocktail of DAPI and anti-Ki67 antibody (1:200, MA514520, ThermoFisher) incubated for 2 h. The chip was washed with 500 μL of PBS via syringe pump, and a secondary antibody (1:500, A-11029, ThermoFisher) was applied overnight. The chip was washed with 500 μL of PBS and imaged immediately.

Fluorescence microscopy was performed on a Zeiss Axio Observer.Z1 microscope equipped with an ORCA-Flash4.0 camera (cat no. C11440−22CU, Hamamatsu). Color images of alcian blue stained monolayers were obtained on an Olympus IX51 microscope equipped with an Olympus DP70 camera.

Confocal microscopy was performed on an LSM 710 confocal microscope (Zeiss) equipped with Zen software (Zeiss) using the Plan-Apochromat 10×/.45 M27 objective. The 405 nm laser was used to excite DAPI. A 512 × 512 pixel scan format was used. Z-slices were acquired at 2.87-μm intervals with each slice representing the average of eight scans.

Statistical Analysis. Student's t test or ANOVA followed by a Tukey's posthoc correction was used to determine statistical significance as indicated in figure legends (error bars indicate standard error of the mean (SEM); p values < 0.05 were considered to be significant).

RESULTS

Cut and Assemble Organ-on-Chips. The bilayer chip presented here (Figure 1a−c) featured apical and basal flow channels interfaced via a PC track etched membrane across a 10 mm length and 1 mm width. The channel height was application dependent. In one embodiment, Caco-2 cells were cultured in a 196 μm tall channel. In a second embodiment to enable monolayer seeding with less concentrated suspensions, primary human intestinal cells were cultured in a 1.6875 mm tall channel. Primary monolayers required seeding cells at a higher cell/cm^2 ratio, which was accomplished by increasing the volume of the cell channel rather than increasing cell concentration. Both apical and basal channels had independent inlets and outlets for cell seeding and medium perfusion. Each bilayer chip consisted of nine discrete layers (Figure 1a) irreversibly bonded to membrane interfaced channels (Figure 1b). While the bilayer chip featured nine layers, each device was constructed in four steps (Figure 1d) to align and bond five components prior to device assembly layer by layer (Figure 1d). To assess the bond strength of tape layers, a single-lap shear test exhibited shear strengths from 0.7 to 1.3 MPa for a small bonded area (1 cm^2) across configurations of MEM, PET, and PMMA (Figure 1e). Laser-cut channels were measured and confirmed to be equivalent to their nominal widths defined in the CAD drawings (Figure S3). Furthermore, adhesive layers displayed minimal compression when stacked (Figure S4), indicating a high stack tolerance for this cut and assembly platform.

Recapitulating the Human Intestine on Cut and Assemble Chips. To initially assess biocompatibility, human intestinal Caco-2 cells were cultured in the cut and assemble bilayer chip under apical and basal medium perfusion. Prior to cell seeding, both channels were coated with rat tail type I collagen to promote cell adhesion. The medium flow rate of 0.84 μL/min delivered a shear stress of 0.015 dyn/cm^2 across the epithelial monolayer as previous work suggested an intestinal lumen shear stress of 0.002−0.08 dyn/cm^2.[28] Caco-2 cells were cultured for 5 days on a chip and compared to cells grown on static Transwell inserts for 5 and 21 days (Figure 2). Transwell controls were included as benchmarks to conventional approaches for polarized cell culture and prior art with bilayer chips fabricated by soft lithography.[11,12,18,59−62] After these time points, the cells were fixed and stained for F-actin, tight junction protein ZO-1, and cell nuclei. Cells formed confluent monolayers with mostly comparable morphology, F-actin expression, and tight junctions under all three culture conditions.

Following initial biocompatibility validation of the cut and assemble bilayer chips, we next assessed cellular function using fluorescent dextran (Figure 3a) and alkaline phosphatase (AP; Figure 3b) and further stained using alcian blue, DAPI, and MUC2 (Figure 3c). Fluorescent dextran (4.4 kDa) transits across a membrane paracellularly, thus by after administering it on the apical end and measuring the apical and basal outlets, the quantified fluorescence (termed "apparent permeability")

https://dx.doi.org/10.1021/acsbiomaterials.0c00190
ACS Biomater. Sci. Eng. 2021, 7, 2949−2963

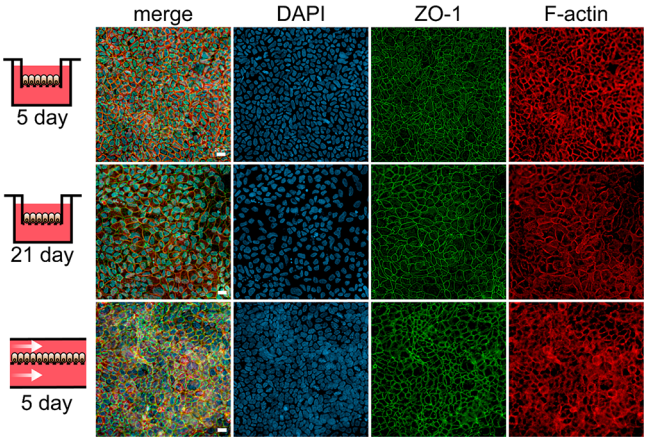

Figure 2. Evaluation of biocompatibility of laser cut and assemble chips. Cell morphology is visualized by immunostaining against ZO-1 tight junctions (green), DAPI nuclei (blue), and F-actin cytoskeleton (red) of Caco-2 cells grown on static Transwell inserts for 5 days (top), 21 days (middle), or on laser cut and assemble chips for 5 days (bottom). Scale bar denotes 20 μm.

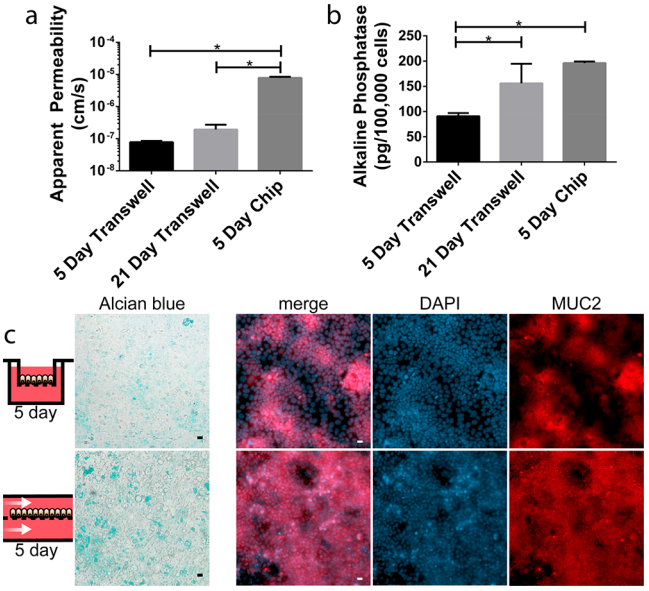

Figure 3. Characterization of epithelial barrier function and Caco-2 monolayer differentiation. (a) The apparent paracellular permeability quantified by tracking a 4.4 kDa fluorescent dextran through Caco-2 monolayers cultured on Transwell inserts for 5 or 21 days and Caco-2 monolayers cultured on a chip for 5 days. Data are presented as mean ± SEM from three independent experiments each utilizing three static inserts and three chips (*p < 0.05 by ANOVA followed by Tukey's HSD test). (b) Alkaline phosphatase expression of Caco-2 cells cultured on Transwell inserts for 5 or 21 days compared to Caco-2 cells cultured on a chip for 5 days. Data are presented as mean ± SEM from three independent experiments each utilizing three static inserts and three chips (* p < 0.05 by ANOVA followed by Tukey's HSD test). (c) Analysis of mucus production by Caco-2 monolayers on Transwell and on a chip. Left-most panels depict representative images of Caco-2 monolayers stained with Alcian Blue. In right-most panels, cells are visualized by DAPI nuclei (blue) staining, and mucus protein is visualized by anti-MUC2 staining (red) of Caco-2 cells grown on static Transwell inserts for 5 days (top) and on laser cut and assembled chips for 5 days (bottom). Scale bars denote 20 μm.

gives a measure of the transport through between the cells.[63] The 5 day chip case demonstrated a significantly higher apparent permeability (p < 0.0001) than both the 5- and 21-day Transwell cultures (Figure 3a). Measurement of alkaline phosphatase (often used to broadly quantify cellular maturity[64−66]) revealed a significantly higher expression (Figure 3b) compared to the 5 day Transwell in the 21 day Transwell (1.7-fold increase with p = 0.0317) and the 5 day chip (2.2-fold increase and p = 0.0035). Further staining using alcian blue (stain for gastrointestinal mucins[67]) and MUC-2 (stain for a gastrointestinal mucosal layer structural protein[68]) indicated increased staining of alcian blue and more uniform MUC-2 in the 5 day chip in comparison to the 5 day Transwell (Figure 3c).

Cut and Assemble Organs-on-Chips Support Primary Human Intestinal Epithelium. We aimed to further asses biocompatibility using the more biorelevant primary intestinal epithelial cells expanded as organoids derived from intestinal biopsies. Alone in Matrigel, the organoids grew in a spheroid morphology (Figure 4a). Once ready for seeding, the organoids were dissociated primarily to single cells (82%; Figure 4b), with 71% viability. Then, cells were plated as a monolayer on either Transwell inserts (Figure 4c) or on cut and assemble chips (Figure 4d) for 5 or 7 days. Phase contrast images were taken at 1, 3, and 5 days of culture on cut and assemble chips (Figure 4d). Static monolayers were maintained in organoid expansion medium (EM) for 2 days followed by differentiation medium (DM) for 5 days while chip monolayers were maintained in EM for 3 days followed by DM for 2 days. Monolayers were then fixed and stained for F-actin, tight junction protein ZO-1, and nuclei (Figure 5a). The stained monolayers demonstrate a similar morphology and confluence between Transwell and cut and assemble cultures. A phase contrast image of the membrane area (Figure 4b) on the chip reveals a similar monolayer health throughout, of which a portion is shown at a higher magnification.

To further evaluate the system, barrier integrity was assessed by measuring the paracellular transport of Lucifer Yellow (450 Da; Figure 5c). We observed a significant increase (p = 0.0029) of about a magnitude (measured in cm/s) in the apparent permeability between the 5-day static and chip models.

Integration of Primary Human Intestinal Monolayers and Intact Organoids in Trilayered Organ Chips. To demonstrate the versatility of the cut and assemble method for multilayered, 3D culture systems, we fabricated architectures in a dual membrane, trilayer organ chip enabling 3D tissue culture (Figure 6a−c) and integrated 2D and 3D tissue culture of primary intestinal monolayers and intact organoids in adjacent compartments. Organoids cultured in standard plasticware thrive throughout approximately 1.5-mm-thick Matrigel (Figure 4a). Therefore, we engineered the trilayer organ chip, again using a layered approach bonded with adhesives, with a 1.6875-mm-tall, central, organoid culture channel (Figure 6c). To promote physical interaction between the differentiated monolayer and the central, organoid laden compartment, the monolayer was cast on a 30 μm pore diameter PC membrane. First, intestinal stem cell laden Matrigel was polymerized in the central channel for 30 min at 37 °C. Then, the apical channel was seeded with dissociated organoids to generate a confluent epithelial monolayer. Organoid expansion medium (EM) was perfused through the apical and basal channels for 6 days. Then, the apical medium was altered to differentiate the epithelial monolayer, and perfusion continued for 4 days. Phase contrast images of

https://dx.doi.org/10.1021/acsbiomaterials.0c00190
ACS Biomater. Sci. Eng. 2021, 7, 2949−2963

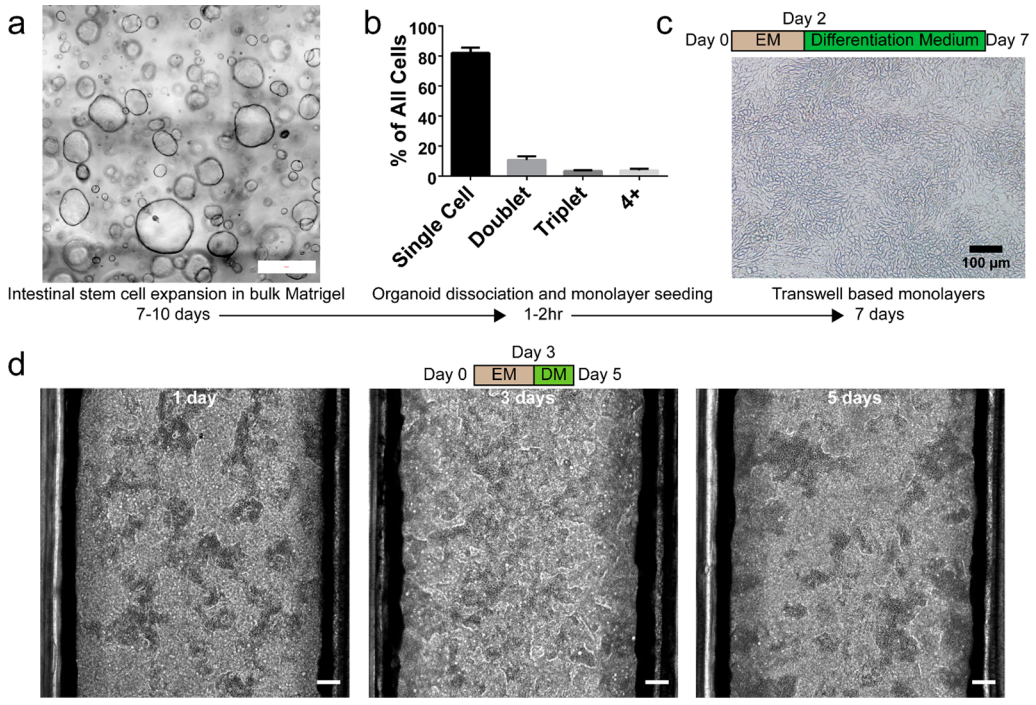

Figure 4. Formation of primary human intestinal monolayers from biopsy-derived organoid cultures. (a) Organoid expansion in 3D Matrigel. Scale bar denotes 500 μm. (b) The percentage of cells/clumps occurring as single cells, doublets, triplets, or clumps of four or more cells after organoid dissociation from three independent experiments. (c) Transwell based monolayers were maintained for 7 days; the phase contrast microscopy image shows Transwell primary human epithelial monolayers at 7 days (note that EM was switched to DM at day 2). (d) Phase contrast images of primary human epithelial monolayers in the bilayer chip at 1, 3, and 5 days post seeding (note that EM was switched to DM at day 3). Scale bar denotes 100 μm.

both the epithelial monolayer and organoid-laden Matrigel were taken at days 2, 4, 6, and 10 (Figure 7). Monolayers achieved confluency in 1−2 days and remained confluent over the 10-day culture duration (Figure 7). Similarly, stem cells formed closed organoids in 1−2 days, which expanded over 10 days and maintained their characteristic cystic morphology (Figure 7). Assessment of the proliferation of the organoid on chip cultures via confocal fluorescence microscopy revealed Ki67+ proliferative stem cells (Figure S1).

At day 10, structural analysis of the system stained with DAPI was conducted using 3D confocal microscopy (Figure 8) and confirmed the presence of single organoids with their characteristic cystic morphology (Figure 8c) as well as larger, morphologically complex organoids (Figure 8d). To analyze Z-depth, monochrome 3D confocal stacks were taken, with each slice colored differentially to represent the z depth. Color coded maximum intensity projections of primary monolayers in the trilayer chip revealed 3D tissue growth spanning approximately 10^2 μm (Figure 8a). Further analysis indicates the location of the organoids within the culture and the changing topography of the monolayer from an orthogonal view (Figure 8b). Orthogonal views of the organoid culture (Figure 8c) indicate some organoids are dwelling on the upper surface of the system in close proximity to the monolayer. A 3D reconstruction of the organoid culture further reveals both a potential interaction of the organoids with the monolayer and the varied landscape of the biological system.

DISCUSSION

Rapid and Facile Cut and Assemble of Bilayer Organs-on-Chips. The cut and assemble manufacturing technique eliminated the PDMS elastomer and micro-fabrication to overcome the aforementioned limitations of soft lithography.[30,34,36] By eliminating lithographic mold fabrication and the subsequent PDMS degassing, curing, and bonding,[9] chips were cut and assembled in approximately 1 h while soft lithography fabrication can span several days.[9] The total material cost per cut and assembled chip was approximately $2 (Table S1). Economical and rapid prototyping is particularly useful in early project phases for iterative design, whereas photomasks may be cost prohibitive ($150−500 per mask depending on feature size), and photo plotting may require several days for turnaround. Furthermore, eliminating lithography enables researchers without micro-fabrication experience or facilities to build organs-on-chips with minimal capital investment. Recent innovative work harnessing 3D printing of molds, versus conventional lithographic measures, minimizes the cost and time significantly for organ-chip fabrication[39] but relies on solution casting of PDMS for channel fabrication, which may not be optimal for certain biological investigations. Our laser cutting system (along with all peripheral equipment including an air compressor and a fume extraction system) cost a total of $12,450, whereas a mask aligner may cost between $30,000−100,000 and does not include peripheral equipment such as a spin coater and vacuum systems. Makerspaces equipped with laser cutters, plotter cutters, and 3D printers further reduce capital costs and increase accessibility.[69] Furthermore, cut and assemble is more amenable to high volume manufacturing techniques such as die cutting, injection molding, and industrial laser cutting as compared to soft lithography.[70] Once a final design iteration is identified via flexible cut and assemble methods at low cost, outsourcing fabrication to

https://dx.doi.org/10.1021/acsbiomaterials.0c00190
ACS Biomater. Sci. Eng. 2021, 7, 2949−2963

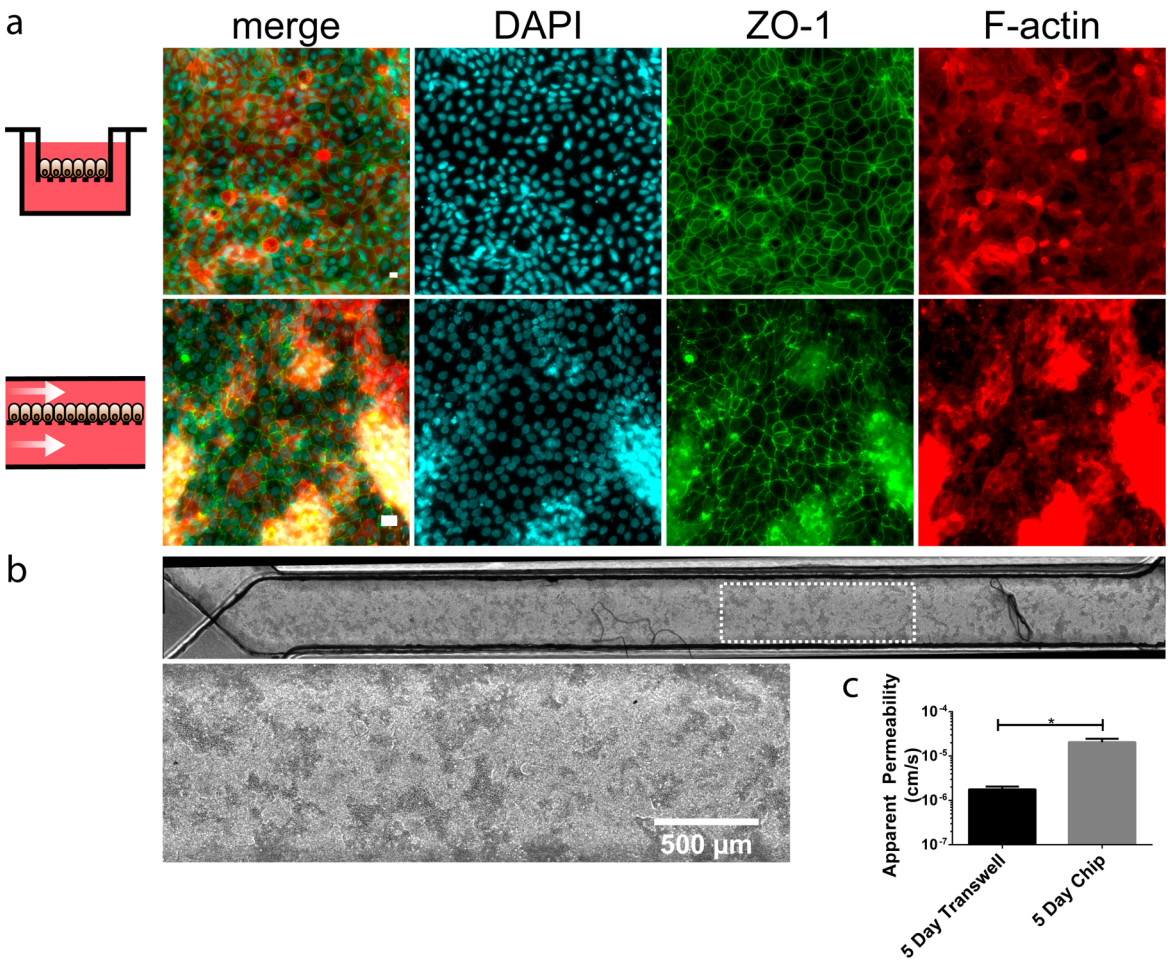

Figure 5. Primary human intestinal epithelium on a chip. (a) Representative images of cells immunostained for ZO-1 tight junctions (green), DAPI nuclei (cyan), and F-actin cytoskeleton (red); primary intestinal cells grown on laser cut and assembled chips for 5 days (bottom) and static inserts for 7 days (top). Scale bar denotes 20 μm. (b) Representative phase contrast images showing primary human epithelium at 5 days across the entire length of the chip and a higher magnification of the area denoted by the white rectangle (bottom, scale bar denotes 500 μm). (c) The apparent paracellular permeability quantified by tracking Lucifer Yellow through primary epithelial monolayers cultured on Transwell inserts or on bilayer chips for 5 days. Data are presented as mean ± SEM from three independent experiments each utilizing three static inserts and three chips generated from organoids isolated from one donor (*p = 0.0029 by Student's t test).

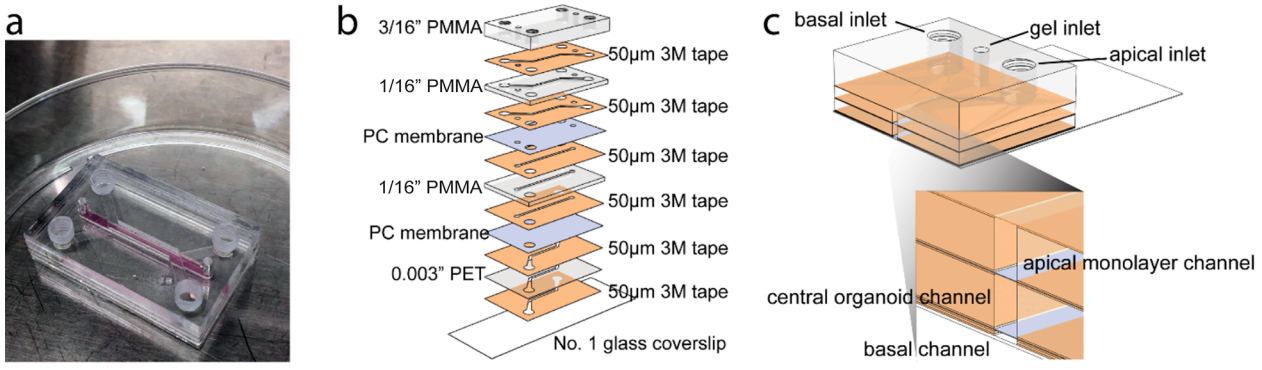

Figure 6. A dual membrane, trilayered organ chip integrating a primary intestinal monolayer and organoids. (a) A photograph of the trilayered organ chip composed of clear PMMA, acrylic adhesive, polycarbonate track etched membranes, and glass coverslip. (b) A schematic showing the integration of 13 discrete layers to form a trilayered chip. (c) A schematic of an assembly cutaway view of the trilayered chip showing the inner apical, central, and basal channels.

commercial MEMs vendors such as Micronit becomes feasible as well.

From a prototyping perspective, the cut and assemble approach's flexibility enables creativity to easily match experimental needs. The channel geometry can be readily modified, and additional channels and membranes can be added or removed. While commercial off the shelf systems for bilayer chips, including primary epithlium,[71] are offered from

https://dx.doi.org/10.1021/acsbiomaterials.0c00190
ACS Biomater. Sci. Eng. 2021, 7, 2949−2963

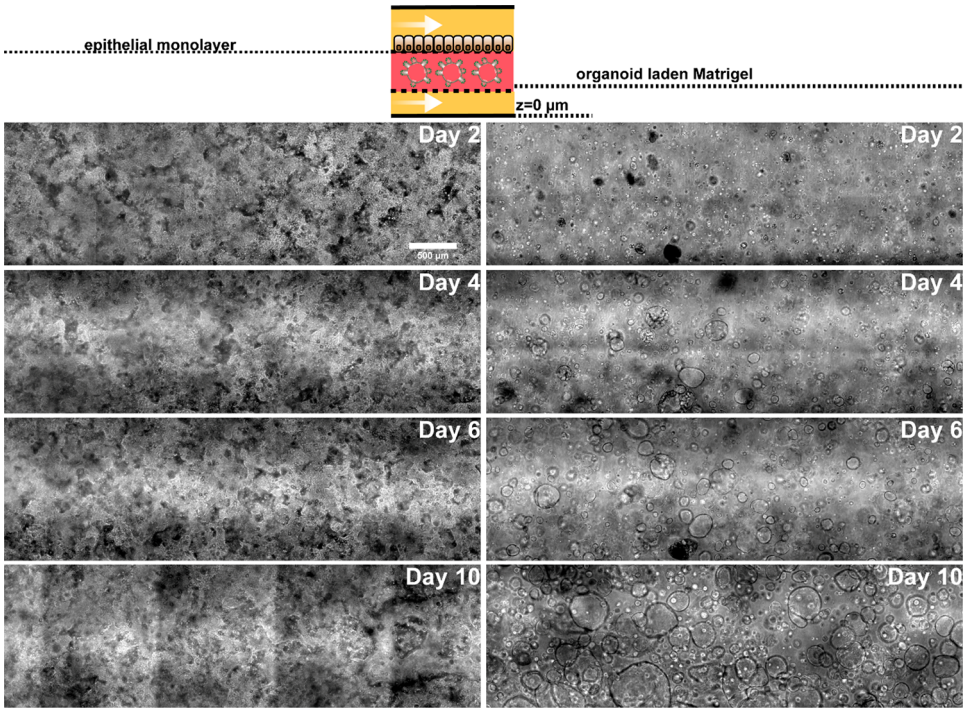

Figure 7. Phase contrast images of primary human epithelial monolayers and organoids in the trilayer chip at 2, 4, 6, and 10 days post seeding (note that apical expansion medium was switched to differentiation medium at day 6). Scale bar denotes 500 μm.

vendors such as Emulate, Inc., the chip geometry is not configurable, chips are made of PDMS,[9] and the full system is cost-prohibitive to many. Substitution of the thickness of the sheets or flow path material enables control in three dimensions. This may be useful when emulating multiple biological barriers such as an epithelium alongside an endothelium.[10]

Though often neglected, facile but reliable fluidic connections simplify chip use, automation, and high-throughput application. Luer Lock and Luer Cone are fluidic interfacing standards but most fabrication techniques, including soft lithography, are incompatible with threaded fluidic connectors. Therefore, we engineered cut and assembled organ chips with threaded ports to accept standard Luer fittings. Cut and assembled organ chips potentially enable O_2 tension control to recapitulate hypoxic tissues because O_2 permeability in acrylic is an order of magnitude lower than PDMS. Similarly, PDMS's high vapor permeability results in significant evaporation relative to the microliter-sized compartments compromising cell viability.[34,12,15,27−29,72]

Under the flow conditions utilized in this work, no chip failure from poor adhesive bonding (leaking, delamination, or bursting) or Luer connections was observed. However, to evaluate the bond strength of our tape layers, a single-lap shear test between our different layered materials was carried out. The assessment (Figure 1e) demonstrated robust structural integrity between the layers (shear strengths of 0.7 to 1.3 MPa depending on the material's structural integrity) with bond strength comparable to two-part epoxy adhesives[73] for the tested overlap area (1 cm^2).

The advantages discussed above are a tradeoff with reduced feature resolution compared to traditional microfabrication. In the $x-y$ plane, soft lithography reliably produces micron-sized features while laser cutting is limited to 10^2 to 10^3 μm. Supporting Information Figure 2 (Figure S2) shows the average deviation of channels cut from the 196-μm-tall bilayer chip channel element (0.003″ PET sheet flanked by 966 adhesive tape on both sides). Note that measurements showed overcutting (positive error) regardless of the nominal channel width. Overcutting may be an effect of the laser spot size during material ablation; the CAD drawing specifies a nominal channel width, but a large laser spot size leads to overcutting past the nominal lines. Furthermore, the results (Figure S2) showed a prohibitively large error (~33% and ~70%) at nominal channel widths of 250 and 125 μm, respectively. However, error was limited to 9.6% and 12.6% for nominal channel widths of 1000 and 500 μm, respectively. These errors may be reduced by compensating for laser overcutting by specifying a nominal channel width of 900 μm to achieve an observed channel width of 1000 μm, for example. While a few previously described tissue chips utilized channel widths less than 500 μm,[9,10,14] channel widths of 1 mm or greater are more frequently used.[9,11,13,15−17] Therefore, we deemed laser cut and assemble suitable for the fabrication of organ chips with channel widths of 500 μm or greater. Further, high performance laser cutters claim a focused spot size of 25 μm, thereby reducing overcutting and approaching lithographic resolutions. Note, however, that laser cutting microfluidic devices introduce error via manual operations such as laser focusing. Additionally, the error may vary depending on the processed material.

In the z plane, traditional microfabrication enables tunable feature height by controlled photoresist deposition. Feature heights of 10^2 to 10^3 μm conventionally require multiple spin coatings and long subsequent baking steps. Theoretically, the minimum cut and assemble feature height is limited to one adhesive tape layer as a channel element, 60 μm in our case, though alternative tapes may be available. Intermediate feature heights are partially constrained; feature height is increased by layering inert thermoplastic materials such as polyester (PET)

https://dx.doi.org/10.1021/acsbiomaterials.0c00190
ACS Biomater. Sci. Eng. 2021, 7, 2949−2963

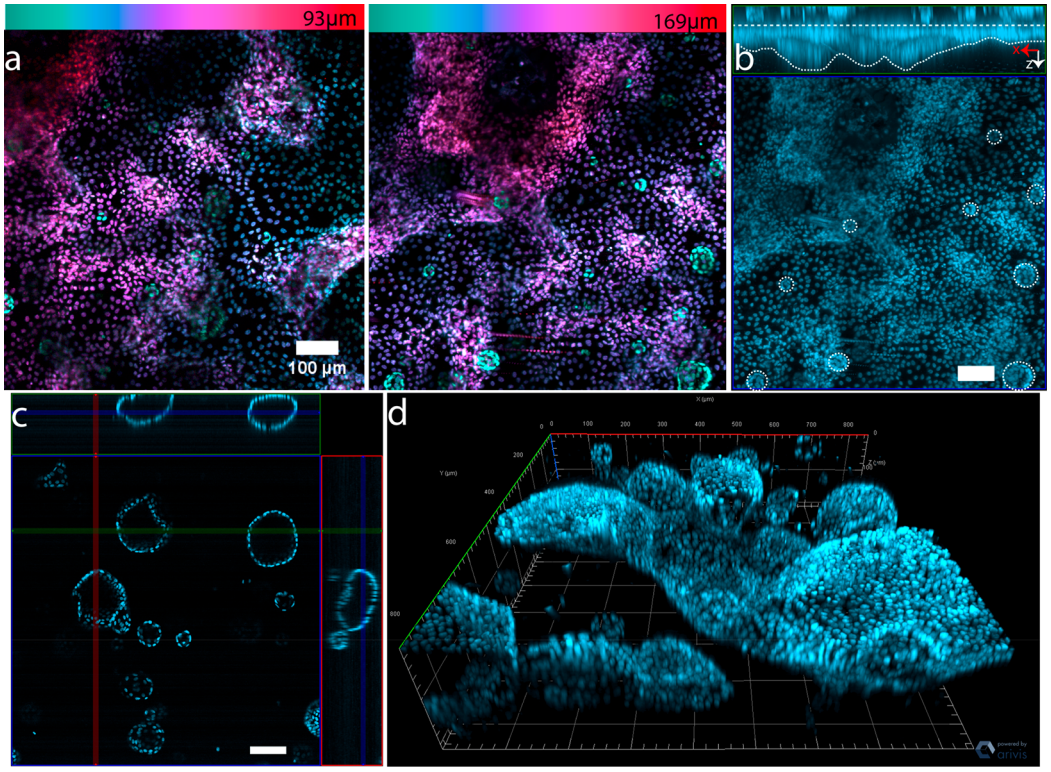

Figure 8. Structural analysis of a dual membrane trilayered organ chip integrating primary human intestinal monolayers and intact organoids. (a) Z-depth color coded maximum intensity projections of the monolayer cultured on chip for 10 days and stained with DAPI when viewed from above by confocal microscopy. The color bars above the image specify the range of z-depths in μm. Both images in panel a were observed on the same chip. (b) A representative maximum intensity z projection and the corresponding orthogonal view of the monolayer cultured for 10 days and stained with DAPI when viewed from above by confocal microscopy. The dashed white lines indicate the upper and lower surfaces of the primary monolayer while the dashed white circles indicate underlying intact organoids in close proximity to the monolayer. (c) Representative orthogonal views of intact organoids cultured on a chip for 10 days, stained with DAPI, and imaged by confocal microscopy. (d) Representative 3D reconstruction of confocal immunofluorescent micrographs of intact organoids cultured on a chip for 10 days and stained for DAPI. Scale bars denote 100 μm.

film between two adhesive tapes. For example, the Caco-2 bilayer chip featured 196-μm-tall channels composed of a 0.003″ PET film sandwiched by two 60 μm adhesive tapes (Figure 4), while the primary cell bilayer chip featured a 1.6875-mm-tall channel composed of a 1/16″ acrylic sheet sandwiched by two 60 μm adhesive tapes (Figure 6). The maximum cut and assemble feature height is theoretically without limits.

Microfluidic Perfusion Culture Impacts Human Intestinal Function in Vitro. The aforementioned bilayer-type chip was evaluated for biocompatibility under perfusion via human intestinal cell cultures. Initially, the Caco-2 cell line (commonly utilized to model for the small intestine) was utilized for basic characterization. Importantly, immunostaining revealed that cells formed confluent monolayers across the integrated membrane (Figure 2) demonstrating the suitability of laser cut or cutter plotter processed adhesives for studying epithelial barrier function. While these technologies were previously used to fabricate microfluidic devices, they were predominantly analytical microfluidic devices,[74−77] with the exception of an organ-on-skin device[78] which used a PDMS cover to facilitate oxygen exchange. This study preliminarily demonstrates that acrylic based adhesives are biocompatible channel elements that support human intestinal epithelial cell culture. Although full analytical testing was not conducted to fully characterize possible toxic residues from laser fabrication, these compounds are likely washed away with vacuum treatment during assembly and subsequent medium perfusion during culture.

Following validation of the biocompatibility of cut and assemble bilayer chips, we next assessed cellular function. As Caco-2 cells cultured on porous membranes are used to model intestinal transport,[11,12,18,59−62,79] we quantified barrier integrity by measuring the apical to basal paracellular transport of a fluorescent dextran (4.4 kDa). Paracellular transport is governed by molecular diffusion through tight junctions rather than active transport via cell membrane bound transporters. The apparent permeability of dextran was calculated as previously described.[80] We did not observe a significant difference (p = 0.9748) between the 5- and 21-day static Transwell models (Figure 3a). Furthermore, the results were consistent with previous permeability measurements of a similarly sized dextran across Caco-2 monolayers.[81−83] In contrast, the apparent permeability across the cut and assemble chip Caco-2 monolayers was 40 and 100 times higher than the static 5-day and 21-day Transwell models, respectively (p < 0.0001; Figure 3a). This finding was unanticipated and may be partly explained by a reduction in boundary layer diffusion resistance due to media perfusion across the cell monolayer, increasing flux at the monolayer surface.[84] The result highlighted the difficulty in comparing monolayer permeability under static and dynamic conditions. Orthogonal measures of paracellular transport which are not influenced via fluid dynamics, such as TEER, may elucidate the differences

https://dx.doi.org/10.1021/acsbiomaterials.0c00190
ACS Biomater. Sci. Eng. 2021, 7, 2949−2963

observed. Further, a direct comparison to prior reports of perfused bilayer organ chips was not included herein, which is a limitation of this work.[11,12,18,59−62]

During extended culture, typically 3 weeks, Caco-2 cells on static Transwell inserts differentiate toward an intestinal enterocyte phenotype expressing transport proteins and brush border enzymes.[44] Among brush border enzymes, alkaline phosphatase (AP) is a frequently used differentiation marker.[64,85,86] As expected, analysis of AP expression revealed a significant 1.7-fold increase ($p = 0.0317$) between Caco-2 on static Transwell inserts at 5 versus 21 days (Figure 3b). However, between Caco-2 cells cultured for 5 days on a chip versus static, AP expression significantly increased 2.2-fold ($p = 0.0035$; Figure 3b). The increased AP expression was consistent with a previous study that reported 4-fold increased AP activity by human proximal tubular epithelial cells in response to perfusion.[87] Perfusion of media may expedite cell differentiation via introduction of flow-induced shear stress, increased exposure to nutrients, and/or decreased exposure to cellular metabolites and waste products compared to static conditions where media is replenished every 48 h.

We next compared mucus production by Caco-2 cells on static Transwell inserts versus a chip. Alcian blue, a polyvalent dye, was used to identify gastrointestinal mucins,[67] and immunostaining was used to specifically identify Mucin 2, the most abundant structural protein of the gastrointestinal mucus layer.[88] Analysis of alcian blue staining suggested that Caco-2 cells on a chip produce more mucus compared cells grown on static Transwells (Figure 3c). These results are consistent with two previous studies combining Caco-2 and other gastrointestinal cell lines with media perfusion that reported increased mucus production in response to mechanical stimulation via fluid flow.[11,89]

While media perfusion may promote cellular differentiation as discussed above, maintaining perfusion via syringe pumps is nontrivial. Syringe pumps placed in incubators generated heat and drove the incubator temperature above 37.0 °C. This was resolved by placing syringe pumps in the incubator the day before cell culture so that the incubators equilibrated back to 37.0 °C. While a syringe pump drove multiple syringes to accommodate multiple chips or channels, all of the syringes output identical flow rates. This imposed limitations in dialing varying volumetric flow rates and/or shear stresses for different channels or parallel chips. Therefore, experiments of varying fluidic conditions cannot be performed in parallel using a single pump.

Introduction of Primary Intestinal Cells from Patient-Derived Organoids. While Caco-2 cells on static permeable supports are frequently used to model enterocytes for transport studies across the small intestinal epithelium, as a model, Caco-2 is limited by its colorectal adenocarcinoma origin. Caco-2 cells contain unknown genetic mutations, fail to fully recapitulate the gut's heterogeneous cell population (stem cells, transit-amplifying cells, Paneth cells, goblet cells, enteroendocrine cells and enterocytes), and may not accurately represent any one cell type. Therefore, we also sought to establish a more physiologically relevant intestine model by utilizing human primary intestinal epithelial cells expanded as organoids derived from intestinal biopsies (Figure 4a). Once broken down into predominantly single cell clusters (Figure 4b), the cells were able to be reseeded as a monolayer (Figure 4c,d).

Immunostaining revealed the primary cells formed confluent monolayers with comparable morphology and tight junctions under both culture conditions (Figure 5a,b), demonstrating suitability for future epithelial barrier studies. We next found that barrier integrity (comparing primary monolayers on chip versus on static inserts) measured by the apical to basal paracellular transport of fluorescent Lucifer Yellow (450 Da) significantly increased ($p = 0.0029$; Figure 5c), consistent with observations for Caco-2 cells (Figure 3a). These results indicate that cut and assemble chips support primary intestinal cells to form confluent monolayers expressing tight junctions and low permeability in response to continuous perfusion.

Inclusion of Intestinal Organoids Promote Growth, Differentiation, and Function of Primary Human Intestinal Monolayers in Trilayered Organ Chips. In the native intestine, epithelial cells are maintained by their surrounding physical, biochemical, and cellular niche.[90] The cellular niche includes myofibroblasts, fibroblasts, endothelial cells, immune cells, glial cells, neural cells, and smooth muscle cells, which are embedded in the ECM underlying the epithelium.[90] The cellular niche regulates epithelial cells via both paracrine and contact dependent signaling.[90] While the bilayer organ chip is the most predominant design, modeling multicellular tissues would benefit from more complex organ chip architectures that enable the integration of more than one to two cell types or 3D tissue culture within a matrix.

While sparse 3D tissue structures spanning a few cell layers were observed in the bilayer organ chip (including both Caco-2 and primary epithelium cultures) (Figure 5a,b), 3D tissue structures in the trilayer organ chip (including a primary epithelium and intestinal organoid coculture) were present across the entire chip length at an even shorter duration of culture (Figure 7). While poor dissociation of primary organoids prior to seeding chips may explain the formation of multicellular structures, these structures were not observed for on Transwells which were dissociated via the same protocols. Increased nutrients due to media perfusion on chip may provide cells the resources for more robust expansion, leading to multicellular tissue structures. Indeed 3D, multicellular, tissue structures on a chip were recently reported and attributed to the presence of media flow and human intestinal microvascular endothelial cells (HIMECs).[13]

Here, we demonstrate 3D tissue growth in the absence of HIMECs. However, the previously reported villus-like structures formed on a collagen I and Matrigel coated membrane. Therefore, it is plausible that biochemical cues originating from laminin and collagen IV rich Matrigel promote 3D tissue growth. In the trilayer chip presented here, tissue growth may be promoted by direct contact between the monolayer and Matrigel through the 30 μm pores as the bilayer chip was only collagen I coated. Confocal fluorescence microscopy revealed organoids in close proximity to the basal regions of the monolayer and 3D tissue structures (Figure 8b). It is possible, though unproven, that intact organoids adjacent to the epithelium communicate with the differentiated epithelial monolayer via paracrine signaling to drive morphological changes. For example, intestinal hedgehog signaling in the intervillous pockets of the developing epithelium is involved in crypt−villus axis formation during development, and the adult small intestine retains Indian Hedgehog (Ihh) ligands in the differentiated villi.[90,91] Thus, integration of the 2D and 3D microenvironments in the trilayer gut chip may exhibit more native functionality of

https://dx.doi.org/10.1021/acsbiomaterials.0c00190
ACS Biomater. Sci. Eng. 2021, 7, 2949−2963

intestinal epithelium and stem cells than independent cultures, while allowing evaluation of monolayer and organoid behavior simultaneously.

Primary monolayers enable intestinal transport studies across an epithelium mainly comprising enterocytes and goblet cells but typically lacking proliferative cell compartments.[53] Conversely, 3D organoids contain proliferative cell compartments but limit intestinal transport study due to poor luminal access. The presence of Ki67+ proliferative stem cells in the cut and assemble organoid culture (Figure S1) demonstrates that the trilayer chip could enable studying intestinal transport across a differentiated epithelium and the subsequent effects on intestinal stem cells. As paracrine Hedgehog signaling between epithelial and mesenchymal cells promotes stromal niche formation which affects epithelial proliferation and differentiation,[90] the trilayer organ chip presented here is a particularly powerful tool for integrating the small intestine's mesenchymal components (fibroblasts, endothelial cells, enteric neurons, and glia) and studying paracrine or cell-to-cell contact-dependent (e.g., enteroendocrine cell-enteric glia[92]) signaling. However, to elucidate interactions between heterogeneous cell types, it should be demonstrated that the cells embedded in the central gel layer can be retrieved for downstream molecular analysis. Otherwise, analysis of the cell culture model presented here would be limited to imaging.

CONCLUSION

Microfabricated organs-on-chips may potentially improve preclinical models, while providing platforms for controlled biological evaluation. In order to gain broad use, organs-on-chips should be simple to use, automated, configurable, and high throughput. Currently, design and redesign can be limited by chip cost, equipment availability, and fabrication complexity. The microfabrication free, cut and assemble manufacturing technique presented herein provides rapid (hours), facile, and inexpensive (~$2 per chip) access to multilayer organs-on-chips with standard fluidic connectors. Caco-2 cells cultured on cut an assemble chips formed confluent monolayers expressing tight junctions, which enabled molecular permeability assays. Caco-2 cells cultured on chips also differentiated ~4 times faster than on Transwell inserts, increasing experimental throughput. The cells on chip also produced mucus and alkaline phosphatase, emulating native intestinal functions. Moreover, cut and assemble chips supported primary human intestinal monolayers with tight junction functional barriers.

The versatility of cut and assemble chips was further demonstrated by generating a dual membrane trilayer gut chip. This trilayer organ chip may be particularly useful for integrating intestinal monolayers with 3D culture of mesenchymal cells (fibroblasts, endothelial cells, enteric neurons, and glial). In a proof-of-principle experiment, we cocultured primary 2D monolayers with 3D organoids. Remarkably, the monolayer formed multicellular 3D structures spanning 10^2 μm, possibly aided by paracrine signaling between the differentiated epithelial monolayer and the proliferative proximate organoids. This platform may enable characterization of intestinal transport and organoid biology toward improved screening and disease modeling, and further design improvements could include enhanced imaging capabilities and increased cell-monolayer interactions. This could be accomplished by decreasing the central channel's height and/or using an apical membrane with pores >30 μm.

The many features of cut and assemble chips, including the low gas and water vapor permeability of thermoplastics, compared to PDMS; the rapid, easy, and economical fabrication method; as well as the ability to make custom multilayered chips, make cut and assemble fabrication well suited for wider adoption and development of organs-on-chips. While laser cut and assembly does not impact the perfusion time limitations nor cell source scaling challenges, the low cost and accessibility of thermoplastic organ chips fabricated by this method may limit design and redesign burden and availability of complex geometries.

ASSOCIATED CONTENT

Supporting Information

The Supporting Information is available free of charge at https://pubs.acs.org/doi/10.1021/acsbiomaterials.0c00190.

Representative 3D reconstruction of confocal immunofluorescent micrographs of intact cultured organoids at 10 days (Figure S1); tensile stress assessment of adhesive bond strength taken to failure (Figure S2); channel stack tolerance post assembly (Figure S4); analysis laser cut variability and tolerance to design (Figure S3); cost analysis of chip fabrication (Table S1) (PDF)

AUTHOR INFORMATION

Corresponding Author

Abigail N. Koppes − *Department of Chemical Engineering and Department of Biology, Northeastern University, Boston, Massachusetts 02115, United States;* orcid.org/0000-0003-0433-9290; Email: a.koppes@northeastern.edu

Authors

Sanjin Hosic − *Department of Chemical Engineering, Northeastern University, Boston, Massachusetts 02115, United States*

Adam J. Bindas − *Department of Chemical Engineering, Northeastern University, Boston, Massachusetts 02115, United States*

Marissa L. Puzan − *Department of Chemical Engineering, Northeastern University, Boston, Massachusetts 02115, United States*

Will Lake − *Department of Chemical Engineering, Northeastern University, Boston, Massachusetts 02115, United States*

Jonathan R. Soucy − *Department of Chemical Engineering, Northeastern University, Boston, Massachusetts 02115, United States*

Fanny Zhou − *Division of Endocrinology, Boston Children's Hospital, Boston, Massachusetts 02115, United States*

Ryan A. Koppes − *Department of Chemical Engineering, Northeastern University, Boston, Massachusetts 02115, United States;* orcid.org/0000-0002-3376-6358

David T. Breault − *Division of Endocrinology, Boston Children's Hospital, Boston, Massachusetts 02115, United States; Department of Pediatrics, Harvard Medical School, Boston, Massachusetts 02115, United States; Principal Faculty, Harvard Stem Cell Institute, Cambridge, Massachusetts 02138, United States*

Shashi K. Murthy − *Department of Chemical Engineering, Northeastern University, Boston, Massachusetts 02115, United States*

Complete contact information is available at:

https://dx.doi.org/10.1021/acsbiomaterials.0c00190
ACS Biomater. Sci. Eng. 2021, 7, 2949−2963

https://pubs.acs.org/10.1021/acsbiomaterials.0c00190

Author Contributions

S.H., A.N.K., and S.K.M. conceived the study. S.H., A.N.K., S.K.M., A.J.B., and R.A.K. provided experimental design input. S.H. conducted the experiments, analyzed the data, and was the primary manuscript author. S.H., M.L.P., W.L., and F.Z. prepared and maintained human organoid cultures. F.Z. and D.T.B. supplied human intestinal tissue for organoid establishment and WRN conditioned medium. A.J.B. conducted mechanical testing, and J.R.S. tolerance testing. All authors provided input toward the manuscript.

Notes

The authors declare no competing financial interest.

■ ACKNOWLEDGMENTS

The authors thank funding support from the National Institute of Health award numbers R21EB025395 Trailblazer (A.K. and R.K.); R01EB021908 BRP (A.K. and D.B.); R01DK084056, P30HD18655, and P30DK034854 (DTB); and the Department of Chemical Engineering at Northeastern University for start-up funding (A.K. and R.K.). Jessica R. Snyder assisted in the editing of this work.

■ REFERENCES

(1) Harrison, R. G.; Greenman, M. J.; Mall, F. P.; Jackson, C. M. Observations of the living developing nerve fiber. *Anat. Rec.* **1907**, *1* (5), 116−128.

(2) Li, Z.; Cui, Z. Three-dimensional perfused cell culture. *Biotechnol. Adv.* **2014**, *32* (2), 243−54.

(3) Maggiorani, D.; Dissard, R.; Belloy, M.; Saulnier-Blache, J. S.; Casemayou, A.; Ducasse, L.; Gres, S.; Belliere, J.; Caubet, C.; Bascands, J. L.; Schanstra, J. P.; Buffin-Meyer, B. Shear Stress-Induced Alteration of Epithelial Organization in Human Renal Tubular Cells. *PLoS One* **2015**, *10* (7), e0131416.

(4) Gayer, C. P.; Basson, M. D. The effects of mechanical forces on intestinal physiology and pathology. *Cell. Signalling* **2009**, *21* (8), 1237−1244.

(5) Powell, D. W.; Mifflin, R. C.; Valentich, J. D.; Crowe, S. E.; Saada, J. I.; West, A. B. Myofibroblasts. II. Intestinal subepithelial myofibroblasts. *Am. J. Physiol.* **1999**, *277* (2), C183−C201.

(6) Yoo, B. B.; Mazmanian, S. K. The Enteric Network: Interactions between the Immune and Nervous Systems of the Gut. *Immunity* **2017**, *46* (6), 910−926.

(7) Huh, D.; Hamilton, G. A.; Ingber, D. E. From 3D cell culture to organs-on-chips. *Trends Cell Biol.* **2011**, *21* (12), 745−54.

(8) Esch, E. W.; Bahinski, A.; Huh, D. Organs-on-chips at the frontiers of drug discovery. *Nat. Rev. Drug Discovery* **2015**, *14* (4), 248−260.

(9) Huh, D.; Kim, H. J.; Fraser, J. P.; Shea, D. E.; Khan, M.; Bahinski, A.; Hamilton, G. A.; Ingber, D. E. Microfabrication of human organs-on-chips. *Nat. Protoc.* **2013**, *8* (11), 2135−57.

(10) Huh, D.; Matthews, B. D.; Mammoto, A.; Montoya-Zavala, M.; Hsin, H. Y.; Ingber, D. E. Reconstituting organ-level lung functions on a chip. *Science* **2010**, *328* (5986), 1662−8.

(11) Kim, H. J.; Ingber, D. E. Gut-on-a-Chip microenvironment induces human intestinal cells to undergo villus differentiation. *Integr Biol. (Camb)* **2013**, *5* (9), 1130−40.

(12) Kim, H. J.; Li, H.; Collins, J. J.; Ingber, D. E. Contributions of microbiome and mechanical deformation to intestinal bacterial overgrowth and inflammation in a human gut-on-a-chip. *Proc. Natl. Acad. Sci. U. S. A.* **2016**, *113* (1), E7−15.

(13) Kasendra, M.; Tovaglieri, A.; Sontheimer-Phelps, A.; Jalili-Firoozinezhad, S.; Bein, A.; Chalkiadaki, A.; Scholl, W.; Zhang, C.; Rickner, H.; Richmond, C. A.; Li, H.; Breault, D. T.; Ingber, D. E. Development of a primary human Small Intestine-on-a-Chip using biopsy-derived organoids. *Sci. Rep.* **2018**, *8* (1), 2871.

(14) Lee, J. S.; Romero, R.; Han, Y. M.; Kim, H. C.; Kim, C. J.; Hong, J. S.; Huh, D. Placenta-on-a-chip: a novel platform to study the biology of the human placenta. *J. Matern.-Fetal Neonat. Med.* **2016**, *29* (7), 1046−54.

(15) Shah, P.; Fritz, J. V.; Glaab, E.; Desai, M. S.; Greenhalgh, K.; Frachet, A.; Niegowska, M.; Estes, M.; Jager, C.; Seguin-Devaux, C.; Zenhausern, F.; Wilmes, P. A microfluidics-based in vitro model of the gastrointestinal human-microbe interface. *Nat. Commun.* **2016**, *7*, 11535.

(16) Torisawa, Y. S.; Spina, C. S.; Mammoto, T.; Mammoto, A.; Weaver, J. C.; Tat, T.; Collins, J. J.; Ingber, D. E. Bone marrow-on-a-chip replicates hematopoietic niche physiology in vitro. *Nat. Methods* **2014**, *11* (6), 663−9.

(17) Sellgren, K. L.; Hawkins, B. T.; Grego, S. An optically transparent membrane supports shear stress studies in a three-dimensional microfluidic neurovascular unit model. *Biomicrofluidics* **2015**, *9* (6), 061102.

(18) Shin, W.; Hinojosa, C. D.; Ingber, D. E.; Kim, H. J. Human Intestinal Morphogenesis Controlled by Transepithelial Morphogen Gradient and Flow-Dependent Physical Cues in a Microengineered Gut-on-a-Chip. *iScience* **2019**, *15*, 391−406.

(19) Edington, C. D.; Chen, W. L. K.; Geishecker, E.; Kassis, T.; Soenksen, L. R.; Bhushan, B. M.; Freake, D.; Kirschner, J.; Maass, C.; Tsamandouras, N.; Valdez, J.; Cook, C. D.; Parent, T.; Snyder, S.; Yu, J.; Suter, E.; Shockley, M.; Velazquez, J.; Velazquez, J. J.; Stockdale, L.; Papps, J. P.; Lee, I.; Vann, N.; Gamboa, M.; LaBarge, M. E.; Zhong, Z.; Wang, X.; Boyer, L. A.; Lauffenburger, D. A.; Carrier, R. L.; Communal, C.; Tannenbaum, S. R.; Stokes, C. L.; Hughes, D. J.; Rohatgi, G.; Trumper, D. L.; Cirit, M.; Griffith, L. G. Interconnected Microphysiological Systems for Quantitative Biology and Pharmacology Studies. *Sci. Rep.* **2018**, *8* (1), 4530.

(20) Jalili-Firoozinezhad, S.; Gazzaniga, F. S.; Calamari, E. L.; Camacho, D. M.; Fadel, C. W.; Bein, A.; Swenor, B.; Nestor, B.; Cronce, M. J.; Tovaglieri, A.; Levy, O.; Gregory, K. E.; Breault, D. T.; Cabral, J. M. S.; Kasper, D. L.; Novak, R.; Ingber, D. E. A complex human gut microbiome cultured in an anaerobic intestine-on-a-chip. *Nature Biomedical Engineering* **2019**, *3* (7), 520−531.

(21) Jeon, J. S.; Bersini, S.; Gilardi, M.; Dubini, G.; Charest, J. L.; Moretti, M.; Kamm, R. D. Human 3D vascularized organotypic microfluidic assays to study breast cancer cell extravasation. *Proc. Natl. Acad. Sci. U. S. A.* **2015**, *112* (1), 214−9.

(22) Adriani, G.; Ma, D.; Pavesi, A.; Kamm, R. D.; Goh, E. L. K. A 3D neurovascular microfluidic model consisting of neurons, astrocytes and cerebral endothelial cells as a blood-brain barrier. *Lab Chip* **2017**, *17* (3), 448−459.

(23) Esch, M. B.; King, T. L.; Shuler, M. L. The role of body-on-a-chip devices in drug and toxicity studies. *Annu. Rev. Biomed. Eng.* **2011**, *13*, 55−72.

(24) Edington, C. D.; Chen, W. L. K.; Geishecker, E.; Kassis, T.; Soenksen, L. R.; Bhushan, B. M.; Freake, D.; Kirschner, J.; Maass, C.; Tsamandouras, N.; Valdez, J.; Cook, C. D.; Parent, T.; Snyder, S.; Yu, J.; Suter, E.; Shockley, M.; Velazquez, J.; Velazquez, J. J.; Stockdale, L.; Papps, J. P.; Lee, I.; Vann, N.; Gamboa, M.; LaBarge, M. E.; Zhong, Z.; Wang, X.; Boyer, L. A.; Lauffenburger, D. A.; Carrier, R. L.; Communal, C.; Tannenbaum, S. R.; Stokes, C. L.; Hughes, D. J.; Rohatgi, G.; Trumper, D. L.; Cirit, M.; Griffith, L. G. Interconnected Microphysiological Systems for Quantitative Biology and Pharmacology Studies. *Sci. Rep.* **2018**, *8* (1), 4530.

(25) Herland, A.; Maoz, B. M.; Das, D.; Somayaji, M. R.; Prantil-Baun, R.; Novak, R.; Cronce, M.; Huffstater, T.; Jeanty, S. S. F.; Ingram, M.; Chalkiadaki, A.; Benson Chou, D.; Marquez, S.; Delahanty, A.; Jalili-Firoozinezhad, S.; Milton, Y.; Sontheimer-Phelps, A.; Swenor, B.; Levy, O.; Parker, K. K.; Przekwas, A.; Ingber, D. E. Quantitative prediction of human pharmacokinetic responses to drugs via fluidically coupled vascularized organ chips. *Nature Biomedical Engineering* **2020**, *4*, 421.

(26) Novak, R.; Ingram, M.; Marquez, S.; Das, D.; Delahanty, A.; Herland, A.; Maoz, B. M.; Jeanty, S. S. F.; Somayaji, M. R.; Burt, M.; Calamari, E.; Chalkiadaki, A.; Cho, A.; Choe, Y.; Chou, D. B.; Cronce, M.; Dauth, S.; Divic, T.; Fernandez-Alcon, J.; Ferrante, T.; Ferrier, J.; FitzGerald, E. A.; Fleming, R.; Jalili-Firoozinezhad, S.; Grevesse, T.; Goss, J. A.; Hamkins-Indik, T.; Henry, O.; Hinojosa, C.; Huffstater, T.; Jang, K.-J.; Kujala, V.; Leng, L.; Mannix, R.; Milton, Y.; Nawroth, J.; Nestor, B. A.; Ng, C. F.; O'Connor, B.; Park, T.-E.; Sanchez, H.; Sliz, J.; Sontheimer-Phelps, A.; Swenor, B.; Thompson, G.; Touloumes, G. J.; Tranchemontagne, Z.; Wen, N.; Yadid, M.; Bahinski, A.; Hamilton, G. A.; Levner, D.; Levy, O.; Przekwas, A.; Prantil-Baun, R.; Parker, K. K.; Ingber, D. E. Robotic fluidic coupling and interrogation of multiple vascularized organ chips. *Nature Biomedical Engineering* **2020**, *4*, 407.

(27) Imura, Y.; Asano, Y.; Sato, K.; Yoshimura, E. A microfluidic system to evaluate intestinal absorption. *Anal. Sci.* **2009**, *25* (12), 1403−7.

(28) Kim, H. J.; Huh, D.; Hamilton, G.; Ingber, D. E. Human gut-on-a-chip inhabited by microbial flora that experiences intestinal peristalsis-like motions and flow. *Lab Chip* **2012**, *12* (12), 2165−2174.

(29) Jang, K. J.; Suh, K. Y. A multi-layer microfluidic device for efficient culture and analysis of renal tubular cells. *Lab Chip* **2010**, *10* (1), 36−42.

(30) Halldorsson, S.; Lucumi, E.; Gomez-Sjoberg, R.; Fleming, R. M. Advantages and challenges of microfluidic cell culture in polydimethylsiloxane devices. *Biosens. Bioelectron.* **2015**, *63*, 218−31.

(31) Zheng, L.; Kelly, C. J.; Colgan, S. P. Physiologic hypoxia and oxygen homeostasis in the healthy intestine. A Review in the Theme: Cellular Responses to Hypoxia. *Am. J. Physiol Cell Physiol* **2015**, *309* (6), C350−60.

(32) Park, T.-E.; Mustafaoglu, N.; Herland, A.; Hasselkus, R.; Mannix, R.; FitzGerald, E. A.; Prantil-Baun, R.; Watters, A.; Henry, O.; Benz, M.; Sanchez, H.; McCrea, H. J.; Goumnerova, L. C.; Song, H. W.; Palecek, S. P.; Shusta, E.; Ingber, D. E. Hypoxia-enhanced Blood-Brain Barrier Chip recapitulates human barrier function and shuttling of drugs and antibodies. *Nat. Commun.* **2019**, *10* (1), 1−12.

(33) Prantil-Baun, R.; Novak, R.; Das, D.; Somayaji, M. R.; Przekwas, A.; Ingber, D. E. Physiologically based pharmacokinetic and pharmacodynamic analysis enabled by microfluidically linked organs-on-chips. *Annu. Rev. Pharmacol. Toxicol.* **2018**, *58*, 37−64.

(34) Heo, Y. S.; Cabrera, L. M.; Song, J. W.; Futai, N.; Tung, Y.-C.; Smith, G. D.; Takayama, S. Characterization and Resolution of Evaporation-Mediated Osmolality Shifts That Constrain Microfluidic Cell Culture in Poly(dimethylsiloxane) Devices. *Anal. Chem.* **2007**, *79* (3), 1126−1134.

(35) Shirure, V.; George, S. Design considerations to minimize the impact of drug absorption in polymer-based organ-on-a-chip platforms. *Lab Chip* **2017**, *17* (4), 681−690.

(36) Aran, K.; Sasso, L. A.; Kamdar, N.; Zahn, J. D. Irreversible, direct bonding of nanoporous polymer membranes to PDMS or glass microdevices. *Lab Chip* **2010**, *10* (5), 548−552.

(37) Hamid, Q.; Wang, C.; Zhao, Y.; Snyder, J.; Sun, W. A three-dimensional cell-laden microfluidic chip for in vitro drug metabolism detection. *Biofabrication* **2014**, *6* (2), 025008.

(38) Hamid, Q.; Wang, C.; Snyder, J.; Williams, S.; Liu, Y.; Sun, W. Maskless fabrication of cell-laden microfluidic chips with localized surface functionalization for the co-culture of cancer cells. *Biofabrication* **2015**, *7* (1), 015012.

(39) Novak, R.; Didier, M.; Calamari, E.; Ng, C. F; Choe, Y.; Clauson, S. L; Nestor, B. A; Puerta, J.; Fleming, R.; Firoozinezhad, S. J; Ingber, D. E Scalable fabrication of stretchable, dual channel, microfluidic organ chips. *J. Visualized Exp.* **2018**, *140*, e58151.

(40) Sundberg, S. O.; Wittwer, C. T.; Gao, C.; Gale, B. K. Spinning disk platform for microfluidic digital polymerase chain reaction. *Anal. Chem.* **2010**, *82* (4), 1546−50.

(41) Kim, J.; Shin, Y.; Song, S.; Lee, J.; Kim, J. Rapid prototyping of multifunctional microfluidic cartridges for electrochemical biosensing platforms. *Sens. Actuators, B* **2014**, *202*, 60−66.

(42) Martínez-López, J. I.; Mojica, M.; Rodríguez, C. A.; Siller, H. R. Xurography as a Rapid Fabrication Alternative for Point-of-Care Devices: Assessment of Passive Micromixers. *Sensors* **2016**, *16* (5), 705.

(43) Stallcop, L. E.; Alvarez-Garcia, Y. R.; Reyes-Ramos, A. M.; Ramos-Cruz, K. P.; Morgan, M. M.; Shi, Y.; Li, L.; Beebe, D. J.; Domenech, M.; Warrick, J. W. Razor-printed sticker microdevices for cell-based applications. *Lab Chip* **2018**, *18* (3), 451−462.

(44) Hubatsch, I.; Ragnarsson, E. G.; Artursson, P. Determination of drug permeability and prediction of drug absorption in Caco-2 monolayers. *Nat. Protoc.* **2007**, *2* (9), 2111−9.

(45) Artursson, P.; Palm, K.; Luthman, K. Caco-2 monolayers in experimental and theoretical predictions of drug transport. *Adv. Drug Delivery Rev.* **2001**, *46* (1−3), 27−43.

(46) Hidalgo, I. J.; Raub, T. J.; Borchardt, R. T. Characterization of the human colon carcinoma cell line (Caco-2) as a model system for intestinal epithelial permeability. *Gastroenterology* **1989**, *96* (3), 736−749.

(47) Delon, L. C.; Guo, Z.; Oszmiana, A.; Chien, C.-C.; Gibson, R.; Prestidge, C.; Thierry, B. A systematic investigation of the effect of the fluid shear stress on Caco-2 cells towards the optimization of epithelial organ-on-chip models. *Biomaterials* **2019**, *225*, 119521.

(48) Sato, T.; Clevers, H. Growing Self-Organizing Mini-Guts from a Single Intestinal Stem Cell: Mechanism and Applications. *Science* **2013**, *340*, 1190−1194.

(49) Leushacke, M.; Barker, N. Ex vivo culture of the intestinal epithelium: strategies and applications. *Gut* **2014**, *63* (8), 1345−54.

(50) Noel, G.; Baetz, N. W.; Staab, J. F.; Donowitz, M.; Kovbasnjuk, O.; Pasetti, M. F.; Zachos, N. C. A primary human macrophage-enteroid co-culture model to investigate mucosal gut physiology and host-pathogen interactions. *Sci. Rep.* **2017**, *7*, 45270.

(51) In, J.; Foulke-Abel, J.; Zachos, N. C.; Hansen, A.-M.; Kaper, J. B.; Bernstein, H. D.; Halushka, M.; Blutt, S.; Estes, M. K.; Donowitz, M.; Kovbasnjuk, O. Enterohemorrhagic Escherichia coli Reduces Mucus and Intermicrovillar Bridges in Human Stem Cell-Derived Colonoids. *Cellular and Molecular Gastroenterology and Hepatology* **2016**, *2* (1), 48−62.

(52) VanDussen, K. L.; Marinshaw, J. M.; Shaikh, N.; Miyoshi, H.; Moon, C.; Tarr, P. I.; Ciorba, M. A.; Stappenbeck, T. S. Development of an enhanced human gastrointestinal epithelial culture system to facilitate patient-based assays. *Gut* **2015**, *64* (6), 911−20.

(53) Wang, Y.; Gunasekara, D. B.; Reed, M. I.; DiSalvo, M.; Bultman, S. J.; Sims, C. E.; Magness, S. T.; Allbritton, N. L. A microengineered collagen scaffold for generating a polarized crypt-villus architecture of human small intestinal epithelium. *Biomaterials* **2017**, *128*, 44−55.

(54) Sidar, B.; Jenkins, B. R.; Huang, S.; Spence, J. R.; Walk, S. T.; Wilking, J. N. Long-term flow through human intestinal organoids with the gut organoid flow chip (GOFlowChip). *Lab Chip* **2019**, *19* (20), 3552−3562.

(55) Lohasz, C.; Rousset, N.; Renggli, K.; Hierlemann, A.; Frey, O. Scalable Microfluidic Platform for Flexible Configuration of and Experiments with Microtissue Multiorgan Models. *SLAS TECHNOLOGY: Translating Life Sciences Innovation* **2019**, *24* (1), 79−95.

(56) Kim, H. J.; Huh, D.; Hamilton, G.; Ingber, D. E. Human gut-on-a-chip inhabited by microbial flora that experiences intestinal peristalsis-like motions and flow. *Lab Chip* **2012**, *12* (12), 2165−74.

(57) Sato, T.; Vries, R. G.; Snippert, H. J.; van de Wetering, M.; Barker, N.; Stange, D. E.; van Es, J. H.; Abo, A.; Kujala, P.; Peters, P. J.; Clevers, H. Single Lgr5 stem cells build crypt−villus structures in vitro without a mesenchymal niche. *Nature* **2009**, *459* (7244), 262−265.

(58) Miyoshi, H.; Stappenbeck, T. S. In vitro expansion and genetic modification of gastrointestinal stem cells as organoids. *Nat. Protoc.* **2013**, *8* (12), 2471−2482.

(59) Maoz, B. M; Herland, A.; FitzGerald, E. A; Grevesse, T.; Vidoudez, C.; Pacheco, A. R; Sheehy, S. P; Park, T.-E.; Dauth, S.; Mannix, R.; Budnik, N.; Shores, K.; Cho, A.; Nawroth, J. C; Segre, D.; Budnik, B.; Ingber, D. E; Parker, K. K. A linked organ-on-chip model

https://dx.doi.org/10.1021/acsbiomaterials.0c00190
ACS Biomater. Sci. Eng. 2021, 7, 2949−2963

of the human neurovascular unit reveals the metabolic coupling of endothelial and neuronal cells. *Nat. Biotechnol.* **2018**, *36* (9), 865−874.
(60) Sontheimer-Phelps, A.; Chou, D. B.; Tovaglieri, A.; Ferrante, T. C.; Duckworth, T.; Fadel, C.; Frismantas, V.; Sutherland, A. D.; Jalili-Firoozinezhad, S.; Kasendra, M.; Stas, E.; Weaver, J. C.; Richmond, C. A.; Levy, O.; Prantil-Baun, R.; Breault, D. T.; Ingber, D. E. Human colon-on-a-chip enables continuous in vitro analysis of colon mucus layer accumulation and physiology. *Cellular and Molecular Gastroenterology and Hepatology* **2020**, *9* (3), 507−526.
(61) Booth, R.; Kim, H. Characterization of a microfluidic in vitro model of the blood-brain barrier (μBBB). *Lab Chip* **2012**, *12* (10), 1784−1792.
(62) van der Helm, M. W.; Henry, O. Y. F.; Bein, A.; Hamkins-Indik, T.; Cronce, M. J.; Leineweber, W. D.; Odijk, M.; van der Meer, A. D.; Eijkel, J. C. T.; Ingber, D. E.; van den Berg, A.; Segerink, L. I. Non-invasive sensing of transepithelial barrier function and tissue differentiation in organs-on-chips using impedance spectroscopy. *Lab Chip* **2019**, *19* (3), 452−463.
(63) Hubatsch, I.; Ragnarsson, E. G. E.; Artursson, P. Determination of drug permeability and prediction of drug absorption in Caco-2 monolayers. *Nat. Protoc.* **2007**, *2*, 2111.
(64) Deng, X.; Zhang, G.; Shen, C.; Yin, J.; Meng, Q. Hollow fiber culture accelerates differentiation of Caco-2 cells. *Appl. Microbiol. Biotechnol.* **2013**, *97* (15), 6943−6955.
(65) Ferruzza, S.; Rossi, C.; Scarino, M. L.; Sambuy, Y. A protocol for differentiation of human intestinal Caco-2 cells in asymmetric serum-containing medium. *Toxicol. In Vitro* **2012**, *26* (8), 1252−1255.
(66) Baltes, S.; Nau, H.; Lampen, A. All-trans retinoic acid enhances differentiation and influences permeability of intestinal Caco-2 cells under serum-free conditions. *Dev., Growth Differ.* **2004**, *46* (6), 503−514.
(67) Matsuo, K.; Ota, H.; Akamatsu, T.; Sugiyama, A.; Katsuyama, T. Histochemistry of the surface mucous gel layer of the human colon. *Gut* **1997**, *40* (6), 782−789.
(68) Schaart, M. W.; Schierbeek, H.; de Bruijn, A. C. J. M.; Tibboel, D.; van Goudoever, J. B.; Renes, I. B. A novel method to determine small intestinal barrier function in human neonates in vivo. *Gut* **2006**, *55* (9), 1366−1367.
(69) Walsh, D. I., 3rd; Kong, D. S.; Murthy, S. K.; Carr, P. A. Enabling Microfluidics: from Clean Rooms to Makerspaces. *Trends Biotechnol.* **2017**, *35* (5), 383−392.
(70) Sackmann, E. K.; Fulton, A. L.; Beebe, D. J. The present and future role of microfluidics in biomedical research. *Nature* **2014**, *507* (7491), 181−9.
(71) Kasendra, M.; Luc, R.; Yin, J.; Manatakis, D. V; Kulkarni, G.; Lucchesi, C.; Sliz, J.; Apostolou, A.; Sunuwar, L.; Obrigewitch, J.; Jang, K.-J.; Hamilton, G. A; Donowitz, M.; Karalis, K. Duodenum Intestine-Chip for preclinical drug assessment in a human relevant model. *eLife* **2020**, *9*, e50135.
(72) Phan, D. T. T.; Wang, X.; Craver, B. M.; Sobrino, A.; Zhao, D.; Chen, J. C.; Lee, L. Y. N.; George, S. C.; Lee, A. P.; Hughes, C. C. W. A vascularized and perfused organ-on-a-chip platform for large-scale drug screening applications. *Lab Chip* **2017**, *17* (3), 511−520.
(73) Balkova, R.; Holcnerova, S.; Cech, V. Testing of adhesives for bonding of polymer composites. *Int. J. Adhes. Adhes.* **2002**, *22* (4), 291−295.
(74) Nath, P.; Maity, T. S.; Pettersson, F.; Resnick, J.; Kunde, Y.; Kraus, N.; Castano, N. Polymerase chain reaction compatibility of adhesive transfer tape based microfluidic platforms. *Microsyst. Technol.* **2014**, *20* (6), 1187−1193.
(75) Sant, H. J.; Gale, B. K. Flexible fabrication, packaging, and detection approach for microscale chromatography systems. *Sens. Actuators, B* **2009**, *141* (1), 316−321.
(76) Crews, N.; Wittwer, C.; Gale, B. Continuous-flow thermal gradient PCR. *Biomed. Microdevices* **2008**, *10* (2), 187−95.
(77) Kim, J.; Surapaneni, R.; Gale, B. K. Rapid prototyping of microfluidic systems using a PDMS/polymer tape composite. *Lab Chip* **2009**, *9* (9), 1290−1293.
(78) Ramadan, Q.; Ting, F. C. W. In vitro micro-physiological immune-competent model of the human skin. *Lab Chip* **2016**, *16* (10), 1899−1908.
(79) Stenberg, P.; Norinder, U.; Luthman, K.; Artursson, P. Experimental and computational screening models for the prediction of intestinal drug absorption. *J. Med. Chem.* **2001**, *44* (12), 1927−37.
(80) Hubatsch, I.; Ragnarsson, E. G. E.; Artursson, P. Determination of drug permeability and prediction of drug absorption in Caco-2 monolayers. *Nat. Protoc.* **2007**, *2* (9), 2111−2119.
(81) Leonard, M.; Creed, E.; Brayden, D.; Baird, A. W. Evaluation of the Caco-2 monolayer as a model epithelium for iontophoretic transport. *Pharm. Res.* **2000**, *17* (10), 1181−8.
(82) Buzza, M. S.; Netzel-Arnett, S.; Shea-Donohue, T.; Zhao, A.; Lin, C. Y.; List, K.; Szabo, R.; Fasano, A.; Bugge, T. H.; Antalis, T. M. Membrane-anchored serine protease matriptase regulates epithelial barrier formation and permeability in the intestine. *Proc. Natl. Acad. Sci. U. S. A.* **2010**, *107* (9), 4200−5.
(83) Cajnko, M. M.; Marusic, M.; Kisovec, M.; Rojko, N.; Bencina, M.; Caserman, S.; Anderluh, G. Listeriolysin O Affects the Permeability of Caco-2 Monolayer in a Pore-Dependent and Ca2+-Independent Manner. *PLoS One* **2015**, *10* (6), e0130471.
(84) Karlsson, J.; Artursson, P. A Method for the Determination of Cellular Permeability Coefficients and Aqueous Boundary-Layer Thickness in Monolayers of Intestinal Epithelial (Caco-2) Cells Grown in Permeable Filter Chambers. *Int. J. Pharm.* **1991**, *71* (1−2), 55−64.
(85) Ferruzza, S.; Rossi, C.; Scarino, M. L.; Sambuy, Y. A protocol for differentiation of human intestinal Caco-2 cells in asymmetric serum-containing medium. *Toxicol. In Vitro* **2012**, *26* (8), 1252−5.
(86) Baltes, S.; Nau, H.; Lampen, A. All-trans retinoic acid enhances differentiation and influences permeability of intestinal Caco-2 cells under serum-free conditions. *Dev., Growth Differ.* **2004**, *46* (6), 503−14.
(87) Jang, K. J.; Mehr, A. P.; Hamilton, G. A.; McPartlin, L. A.; Chung, S.; Suh, K. Y.; Ingber, D. E. Human kidney proximal tubule-on-a-chip for drug transport and nephrotoxicity assessment. *Integr Biol. (Camb)* **2013**, *5* (9), 1119−29.
(88) Schaart, M. W.; Schierbeek, H.; de Bruijn, A. C.; Tibboel, D.; van Goudoever, J. B.; Renes, I. B. A novel method to determine small intestinal barrier function in human neonates in vivo. *Gut* **2006**, *55* (9), 1366−7.
(89) Navabi, N.; McGuckin, M. A.; Linden, S. K. Gastrointestinal cell lines form polarized epithelia with an adherent mucus layer when cultured in semi-wet interfaces with mechanical stimulation. *PLoS One* **2013**, *8* (7), e68761.
(90) Meran, L.; Baulies, A.; Li, V. S. W. Intestinal Stem Cell Niche: The Extracellular Matrix and Cellular Components. *Stem Cells Int.* **2017**, *2017*, 7970385.
(91) van den Brink, G. R. Hedgehog signaling in development and homeostasis of the gastrointestinal tract. *Physiol. Rev.* **2007**, *87* (4), 1343−75.
(92) Bohórquez, D. V.; Samsa, L. A.; Roholt, A.; Medicetty, S.; Chandra, R.; Liddle, R. A. An Enteroendocrine Cell − Enteric Glia Connection Revealed by 3D Electron Microscopy. *PLoS One* **2014**, *9* (2), e89881.

https://dx.doi.org/10.1021/acsbiomaterials.0c00190
ACS Biomater. Sci. Eng. 2021, 7, 2949−2963